CHAPTER 2

Microdrops

2.1 Introduction

In Chapter 1, we dealt with microflows. Another aspect of microfluidics is the physics of microdrops. Microdrops are a common feature in biotechnology. For example, DNA microarrays are comprised of hundreds to thousands of microwells, each containing a drop of biologic liquid, and a drop dispenser is used to deposit the liquid in each well (Figure 2.1). In such a case, it is essential to understand how the drop relocates in a well.

Another relatively new concept in microfluidics is the use of microdrops to perform the same bioanalysis and biorecognition operations as classical microflows devices do. There are some arguments about whether it is better to use microflows or microdrops in microsystems for biotechnology. The choice is complex because it depends on many factors.

First, microflows are more commonly used, better known, and more familiar to the developers. Micropumps and microvalves are now available, and microchannel etching in silicon, plastic, or glass is now a standard technique. Second, microdrop behavior is often complex and puzzling—as we shall see in this chapter. However, microdrops have the big advantage of minimizing the surface between the liquid and the solid walls. In biotechnology, it is a real advantage since "nonspecific" adsorptions—contact and adherence of the target particles on solid walls at unwanted places in the microsystem—are a constant drawback. If these particles are marked with a fluorescent marker, they constitute a perturbing light source that hampers the detection of the real signal. Another advantage of microdrops in biology is that it is possible to work with very small amounts of liquid, much smaller than it is possible to use in classical microflows. In electrowetting devices, for example, the volume of the drops may be as low as 0.05 μl. Finally, assuming that the technique to move and control microdrops on a plane surface is mastered, fluidic tracks that resemble the one used to define conducting paths on an electronic semiconductor device may be built (Figure 2.2). One sometimes refers this approach as *digital* or *flatland microfluidics*.

On the other hand, microdrop technology is not adapted to all situations, such as the continuous analysis of large volumes of liquids. Microdrops are not going to replace continuous flow processes but rather complete the panel of existing devices to tackle the many facets of biotechnology.

In this chapter, we deal first with the basic notions of the physics of wetting in order to familiarize the reader with the mechanical behavior of interfaces. Then we will focus on the physics of drops with the important notions of minimal surface

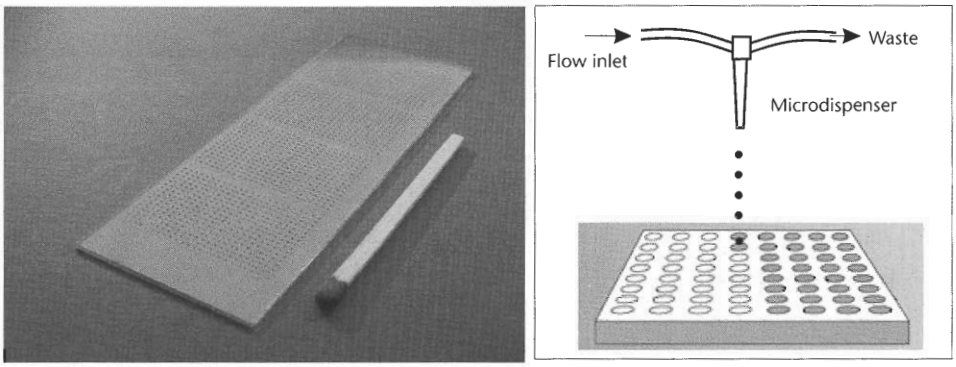

Figure 2.1 (Left) DNA microarray made by SCIENION; and (right) the principle of microdispensing of liquid into wells of a microplate.

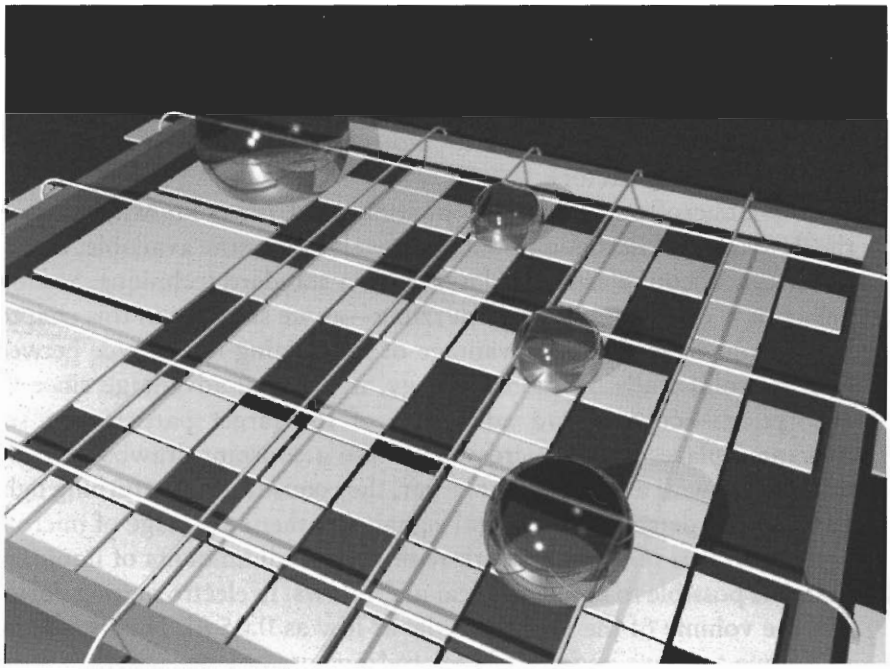

Figure 2.2 Schematic view of a concept of a microdevice using microdrops. (Courtesy of CEA/LETI.)

and contact forces. Finally, we give an example of application of flatland/digital microfluidics using the principle of electrowetting.

2.2 The Physics of Wetting

2.2.1 Capillarity: Surface Tension and Contact Angles

2.2.1.1 Interfaces and Surface Tension

Mathematically speaking, an interface is the geometrical surface that delimitates two fluid domains. This definition implies that an interface has no thickness and is

smooth (i.e., it has no roughness). As practical as it is, this definition is in reality a schematic concept. The reality is more complex, and the separation of two immiscible fluids (water/air, water/oil, and such) depends on molecular interactions between the molecules of each fluid [1]. A microscopic view of the interface between two fluids looks more like the scheme of Figure 2.3.

However, as it has been mentioned earlier, even for microdrops, we are more interested in the macroscopic behavior of the interface, and the mathematical concept regains its utility. The former picture can be viewed at a macroscopic size, as shown in Figure 2.4.

In a condensed state, molecules attract each other. Molecules located in the bulk of a liquid have interactions with all neighboring molecules; these interactions are mostly Van der Waals attractive interactions for organic liquids and hydrogen bonds for polar liquids like water. On the other side, molecules at an interface have interactions in one half space with molecules of the same liquid and in the other half space interactions with the molecules of the other fluid or gas (Figure 2.5).

Suppose an interface between a liquid and a gas. In the bulk of the liquid, a molecule is in contact with 4 to 12 other molecules, depending on the liquid (4 for water and 12 for simple molecules); at the interface this number is divided by two. Of

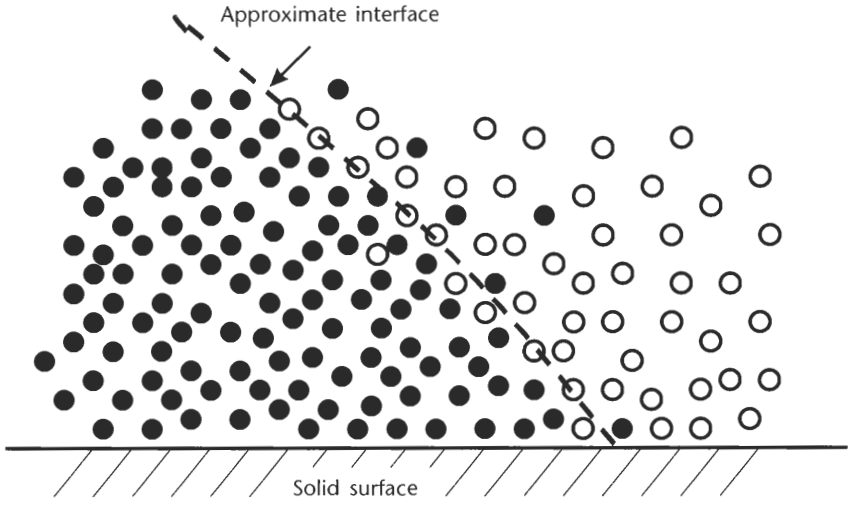

Figure 2.3 Schematic view of an interface at the molecular size.

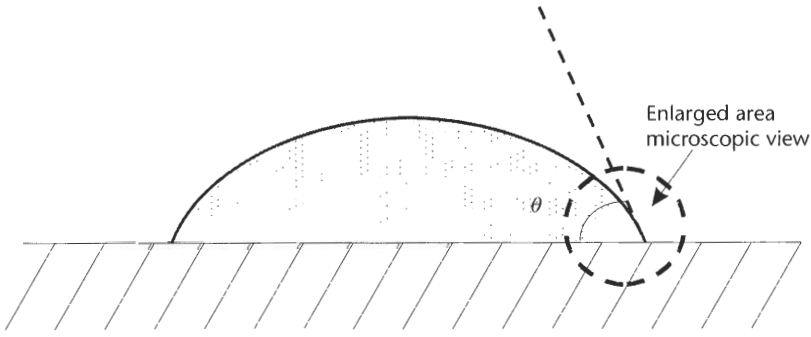

Figure 2.4 Macroscopic view of the interface of a drop.

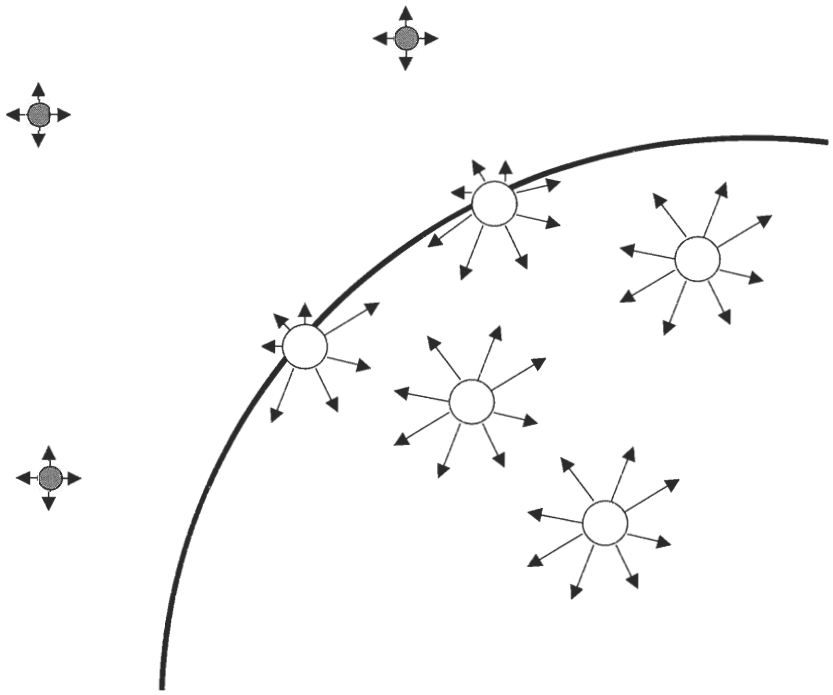

Figure 2.5 Simplified scheme of molecules near an air/water interface. In the bulk, molecules have interaction forces with all of the neighboring molecules. At the interface, half of the interactions have disappeared.

course, the molecule is also in contact with gas molecules, but, due to the low densities of gases, there are less interactions and less interaction energy than in the liquid side. The result is that there is locally a dissymmetry in the interactions, which results in a defect of surface energy.

The same reasoning applies to the interface between two liquids, except that the interactions with the other liquid will usually be more energetic than a gas and the resulting dissymmetry will be less. For example, we will see in Table 2.1 that the contact energy (surface tension) between water and air is 72 mN/m, whereas it is only 50 mN/m between water and oil.

It is also the same for a solid and a liquid. The interface is just the physical contact surface. Molecules in the liquid are attracted toward the interface by Van der Waals forces. But usually these molecules do not "stick" at the wall because of Brownian motion. However, impurities contained in the fluid, like particles of dust or biological polymers like proteins, may well adhere permanently to the solid surface because, at the contact with the solid interface, they experience more attractive interactions. This is because the size of polymers is much larger than that of water molecules, and Van der Waals forces are proportional to the number of contacts.

Table 2.1 Typical Values of Surface Tensions at Room Temperature

Type of Components	*Water/Air*	*Water/Oil*	*Glycerol/Air*	*Ethanol/Air*	*Cyclohexan/Air*	*Mercury/Air*
Surface tension [mN/m]	72	50	63	23	25	485

Source: [2].

At the macroscopic scale, a physical quantity called *surface tension* has been introduced in order to take into account this molecular effect. The surface tension has the dimension of energy per unit surface, and in the International System it is expressed in J/m^2 or N/m (sometimes it is more practical to use mN/m as a unit for surface tension): it is the local defect of energy at the interface divided by the area occupied by a molecule.

In the literature or on the Internet there exist tables for surface tension values [3, 4]. Typical values of surface tensions are given in Table 2.1.

Usually surface tension is denoted by the Greek letter γ, with subscripts referring to the two components on each side of the interface (e.g., γ_{LG} at a liquid/gas interface). Most of the time, if the contact is with air, the subscripts are omitted.

Just because of the definition of the surface tension, for a homogeneous interface (same molecules at the interface all along the interface), the total energy of the surface is

$$E = \gamma S \tag{2.1}$$

2.2.1.2 Capillary Forces

Surface tension can be looked at as a force per unit length. This can be directly seen from its unit since surface tension is expressed in N/m, which is indeed a force per unit length. But it may be interesting to give a more physical feeling by doing a very simple experiment (Figure 2.6) [2]. Take a solid frame and a solid tube that can roll on this frame. If we form a liquid film of soap between the frame and the tube by plunging one side of the structure in a water-soap solution, the tube starts to move toward the region where there is the liquid film. The surface tension of the liquid film exerts a force on its free boundary.

On the other hand, we can increase the film surface by exerting a force on the tube. The work of this force is given by the relation

$$\delta W = Fdx = 2\gamma L dx$$

The coefficient 2 stems from the fact that there are two interfaces between the liquid and the air. This relation shows that the surface tension γ is a force per unit length, perpendicular to the tube, in the plane of the liquid and directed toward the liquid.

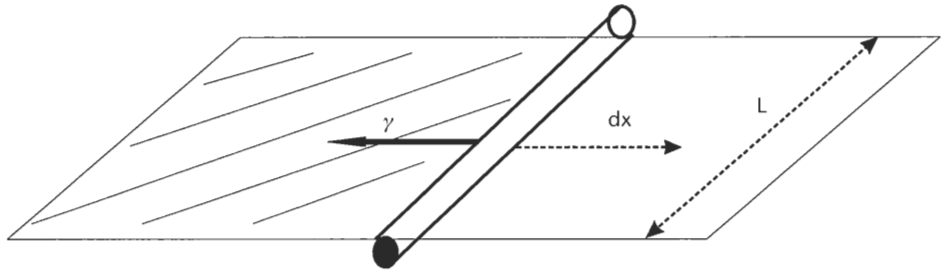

Figure 2.6 A tube placed on a rigid frame where the left part is occupied by a film of glycerin displaced toward the left.

Capillary forces are extremely important at a microscale. For example, it is very difficult to separate two parallel plates separated by a liquid film.

2.2.2 Wetting: Young's Law

The behavior of microdrops on a solid surface is of utmost importance for the conception of microsystems in biology. This solid surface may be the tip of a microneedle or a micropipette; it may be the surface of a microplate with thousands of cusps or that of a Teflon-coated electrowetting device. In any case, we need know the behavior of the drop. The microdrop must detach easily from the tip of the pipette or the needle, stay in the microcusps without flowing by capillarity inside the other neighboring cusps to avoid biological contamination, or follow the electrodes line of the electrowetting device.

Wetting characterizes the contact of a liquid with a solid surface. Generally speaking, there are two types of wetting: total and partial. Total wetting corresponds to the case where a liquid film spreads out on the solid surface, and partial wetting occurs when the liquid stays in drops, as shown in Figure 2.7.

A criterion for total wetting is given by the spreading coefficient S given by

$$S = \gamma_{SG} - (\gamma_{SL} + \gamma_{LG})$$

If S is positive, the drop spreads on the solid surface as a liquid film. If S is negative, it is a situation of partial wetting. In the case of partial wetting, there is a line where all three phases come together. This line is called the *contact line* or sometimes the *triple line*. The contact of a water droplet on a solid is said to be hydrophilic or hydrophobic, depending on the contact angle (Figure 2.8).

We have seen that surface tensions are not exactly forces; their unit is N/m; however, they represent a force that is exerted tangentially to the interface. We can then draw the different forces that are exerted by the presence of a fluid on the triple line (Figure 2.9).

Note that we have noted the wall characteristics by the terms *hydrophilic* or *hydrophobic* with reference to water. In general, we should say that a liquid is "wetting" or "not wetting" a specific surface based on the contact angle of a drop with the surface.

A criterion of wetting may be derived from surface tension considerations: At equilibrium, the resultant of the forces must be zero. We use a coordinate system

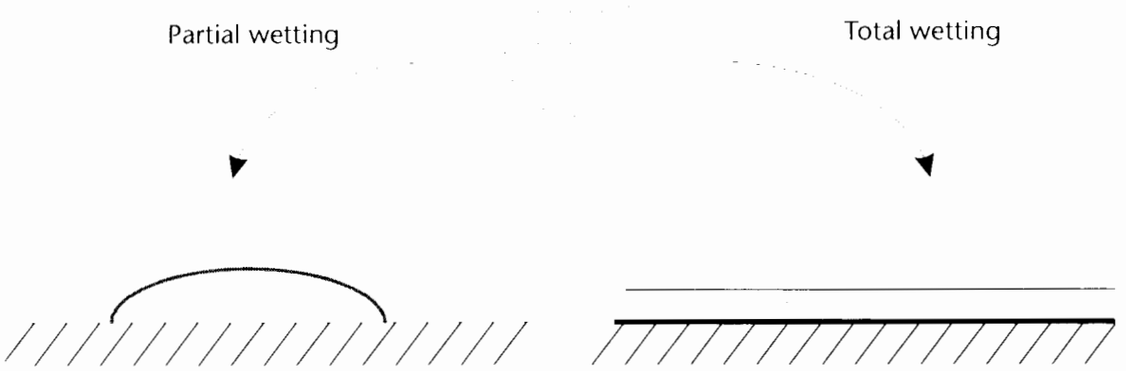

Figure 2.7 Partial wetting and total wetting.

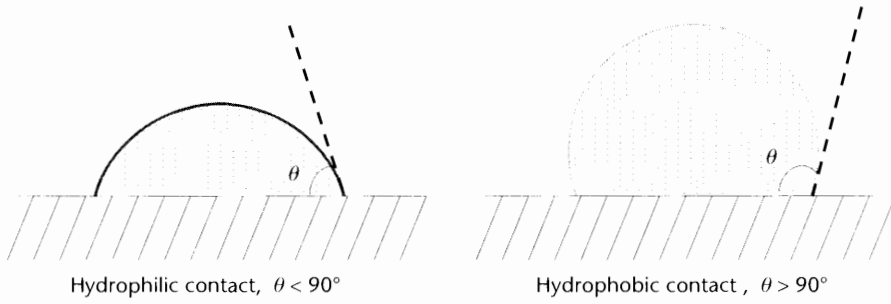

Figure 2.8 Hydrophilic and hydrophobic contact.

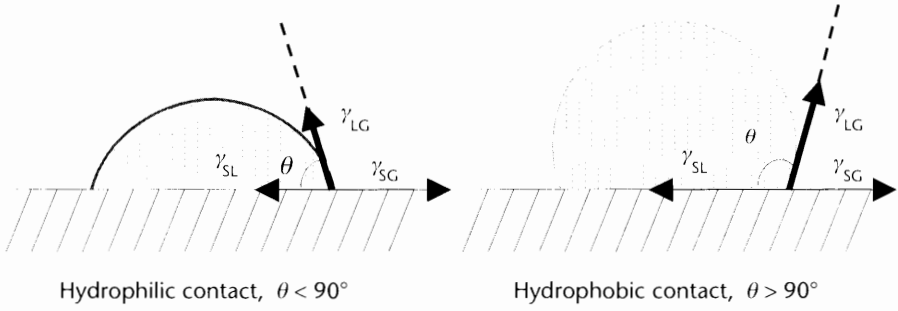

Figure 2.9 Schematic view of the forces at the triple line.

where the x-axis is the tangent to the solid surface at the contact line (in the Figure 2.9 it is horizontal) and the y-axis is the direction perpendicular (vertical). Then the projection of the resultant on the x-axis is zero, and we obtain the relation

$$\gamma_{LG} \cos\theta = \gamma_{SG} - \gamma_{SL} \tag{2.2}$$

This relation is called Young's law and is very useful to understand the behavior of a drop. In particular, it shows that the contact angle is determined by the surface tensions of the three constituents. For a microdrop on a solid, the contact angle is given by the relation

$$\theta = \arccos \frac{\gamma_{SG} - \gamma_{SL}}{\gamma_{LG}}$$

Sometimes in real experimental situations, when we deal with real biological liquids, one observes an unexpected change in the contact angle with time. This is just because biological liquids are inhomogeneous and can deposit a layer of chemical molecules on the solid wall, thus progressively changing the value of the tension γ_{SL}, and consequently the value of θ, as it is stated by Young's law.

One may note that Young's law was obtained by a projection of the forces on the x-axis, but what about the projection on the y-axis? As a matter of fact, there is a vertical force acting on the solid surface and directed away from the solid. It is balanced by the reaction of the solid. If the solid is replaced by a liquid $L2$ nonmiscible with the liquid $L1$ (e.g., oil and water), as shown in Figure 2.10, then the surface is

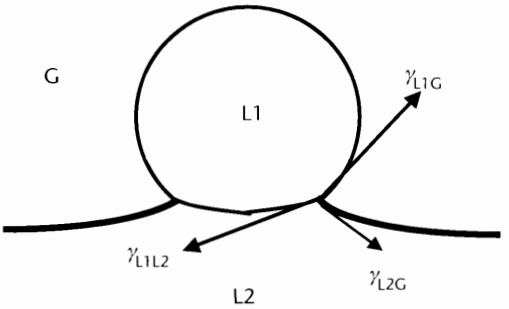

Figure 2.10 Schematic view of a microdrop of oil on top of a water layer. Because of its small dimension, the shape of the drop in the air is spherical. At the triple line, Young's law applies and the resultant of the forces is zero.

distorted so that the resultant of the forces at the triple line is zero. The resultants of the projections of the forces are zero as well on the x-axis and y-axis.

If the dimension of the drop is larger, the contact would be similar, but the shape of the interfaces would be somewhat nonspherical due to the gravitational forces, as shown in Figure 2.11.

Note that there is a singular point at the triple line: the vectors γ_{L1L2} and γ_{L2G} are not collinear, because if they were, the resultant of the forces would not be zero.

Another very interesting derivation of Young's law was done by Shapiro and coworkers [5]. Instead of considering forces at the triple line, Shapiro uses the principle of minimal energy for a drop at equilibrium. Take the example of a sessile drop placed on a horizontal plane (Figure 2.12) and suppose that the dimensions of the drop are small enough so that gravitational forces can be neglected (we will later give a justification for neglecting gravity effect on microdrops), the shape of the drop is then spherical. Due to this spherical shape, the drop volume is a function of R and θ. According to the notations of Figure 2.12, the drop characteristic dimensions h (drop height) and a (drop contact radius) are

$$h = R(1 - \cos\theta)$$

and

$$a = R\sin\theta$$

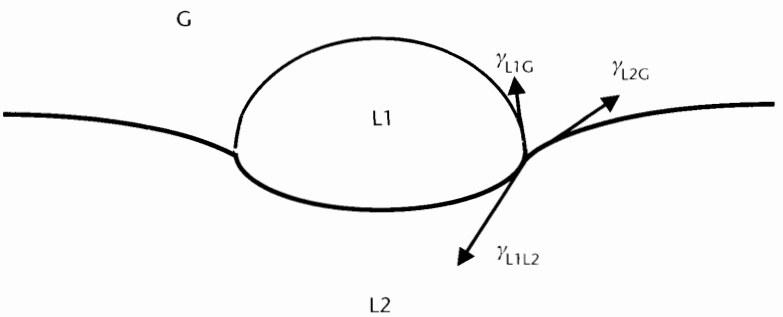

Figure 2.11 Schematic view of a drop of liquid *L1* (oil) deposited on liquid *L2* (water).

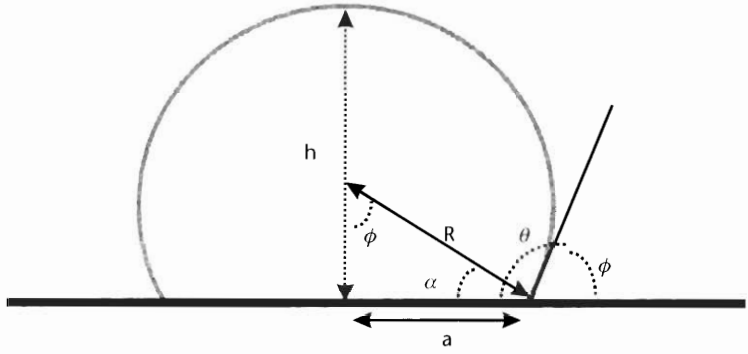

Figure 2.12 Schematic view of a microdrop sitting on a horizontal plane.

The drop volume is then [6]

$$V = \frac{\pi}{3} R^3 \left(2 - 3\cos\theta + \cos^3\theta\right) = \frac{\pi}{3} a^3 \frac{\left(2 - 3\cos\theta + \cos^3\theta\right)}{\sin^3\theta} \tag{2.3}$$

The volume V can be cast into the form

$$V = \pi R^3 \left(\frac{2}{3} - \frac{3\cos\theta}{4} + \frac{\cos 3\theta}{12}\right)$$

Using the principle of minimal energy at equilibrium, and noting that the energy is a function of the two parameters R and θ,

$$E = E(R, \theta)$$

one obtains the following relation

$$dE = \frac{\partial E}{\partial R}(R, \theta) dR + \frac{\partial E}{\partial \theta}(R, \theta) d\theta = 0 \tag{2.4}$$

Since the volume of the drop is constant, its variation must be zero, hence

$$dV = 3\pi R^2 \left(\frac{2}{3} - \frac{3\cos\theta}{4} + \frac{\cos 3\theta}{12}\right) dR + \pi R^3 \left(\frac{3\sin\theta}{4} - \frac{\sin 3\theta}{4}\right) d\theta = 0$$

This later relation can be cast under the form

$$dR = R \left(-\frac{2\cos^2\left(\frac{\theta}{2}\right)\cot\left(\frac{\theta}{2}\right)}{2 + \cos\theta}\right) d\theta = R\, q(\theta) d\theta \tag{2.5}$$

Equation (2.5) can be substituted in (2.4) and we find

$$\frac{\partial E}{\partial R}(R,\theta)Rq(\theta)+\frac{\partial E}{\partial \theta}(R,\theta)=0 \tag{2.6}$$

We show now that (2.6) is the Young equation (2.2) written in another form. In this case, where the energy of the drop is only due to solid/liquid, solid/gas, and liquid/gas interfaces, the total energy is

$$E=(\gamma_{LS}-\gamma_{GS})S_{LS}+\gamma_{LG}S_{LG} \tag{2.7}$$

In (2.7), S denotes the surface. Note that the solid/gas coefficient is negative because if S_{LS} is increased by some amount, then S_{GS} must be decreased by the same amount. Because the drop has a spherical shape, the surfaces appearing in (2.7) are functions of R and θ. Using the expression of the volume of the spherical cap (2.3) and the expression for the contact radius a, we find the following expressions for the contact and free surfaces

$$\begin{aligned} S_{LS} &= \pi R^2 \sin^2\theta \\ S_{LG} &= 2\pi R^2(1-\cos\theta) \end{aligned} \tag{2.8}$$

In consequence, the interfacial energy is

$$E=\pi R^2\left[(\gamma_{LS}-\gamma_{GS})\sin^2\theta+2\gamma_{LG}(1-\cos\theta)\right] \tag{2.9}$$

If we differentiate E relative to R and to θ, and plug the result into (2.6), we obtain exactly, after some trigonometric algebra, Young's law.

This energy approach may seem more complicated than the direct approach using the force balance at the triple line, but it is very powerful because it is more generic, as we shall see in Section 2.2.8.

2.2.3 Wenzel's Law

Let's come back to a contact between a liquid drop and a solid. Roughness of the solid walls modifies the contact between the liquid and the solid. But the effect of roughness on the contact angle is not intuitive. It is a surprising but very useful observation that roughness amplifies the character hydrophilic or hydrophobic of the contact.

Suppose that θ is the angle with the surface with roughness and θ^* is the angle with the smooth surface (in both cases, the solid, liquid, and gas are the same). One very important point here is that we have made the implicit assumption that the size of the roughness is very small, so that the molecules of the liquid are interacting macroscopically with a plane surface but microscopically with a rough surface. This explains why we can use the unique angle of contact θ. As a general rule, the size of the roughness should be smaller than the mean interaction distance between liquid molecules and the solid wall.

Suppose a very small displacement of the contact line (Figure 2.13). Then the work of the different forces acting on the contact line is given by

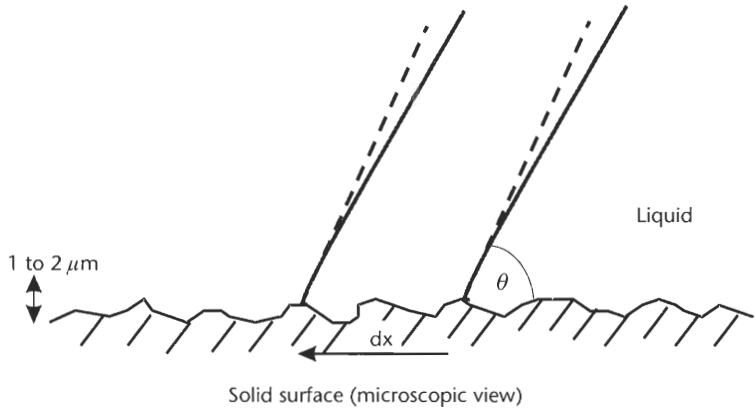

Figure 2.13 Contact of a liquid drop on a rough surface.

$$dW = \sum \vec{F} \cdot \vec{dl} = \sum F_x dx = (\gamma_{SL} - \gamma_{SG})rdx + \gamma_{LG} \cos\theta dx \tag{2.10}$$

where r is the roughness ($r\,dx$ is the real distance on the solid surface when the contact line is displaced of dx). Note that by definition, $r > 1$. Thus, the change in energy is

$$dE = dW = (\gamma_{SL} - \gamma_{SG})rdx + \gamma_{LG} \cos\theta dx \tag{2.11}$$

In fact, if we imagine that the drop finds its equilibrium state after the small perturbation dx, it finally stops at a position where its energy is minimum, so that

$$\frac{dE}{dx} = 0$$

and we obtain the relation

$$\gamma_{LG} \cos\theta = (\gamma_{SG} - \gamma_{SL})r \tag{2.12}$$

If we recall that Young's law is for a smooth surface

$$\gamma_{LG} \cos\theta^* = \gamma_{SG} - \gamma_{SL}$$

then we obtain Wenzel's law

$$\cos\theta = r\cos\theta^* \tag{2.13}$$

Taking into account that $r > 1$, this relation implies that

$$|\cos\theta| > |\cos\theta^*| \tag{2.14}$$

We can deduce that if θ^* is larger than 90° (hydrophobic contact), then $\theta > \theta^*$, and the contact is still more hydrophobic due to the roughness. If θ^* is smaller than 90° (hydrophilic contact), then $\theta < \theta^*$, and the contact is still more hydrophilic due to the roughness.

An important remark at this stage is that the scale of the roughness on the solid surface is *very small compared to that of the drop* [7]. Indeed, if not, it would not be possible to define a unique contact angle anymore; the drop would no longer be axisymmetrical, and the contact could be sketched as in Figure 2.14 (the position of the drop might not be stable).

2.2.4 Superhydrophobicity and Superhydrophilicity

Wenzel's law is in part only the explanation to the so-called superhydrophilic or superhydrophobic contact. According to Wenzel's law, hydrophobicity or hydrophilicity is enhanced by an increase of the surface roughness. However, to obtain superhydrophobicity, the roughness must be increased in such a way that air is trapped in the porosities or rugosities underneath the droplet.

In nature, some plants living in a very wet environment have leaves with such roughness that raindrops just roll along their surface without any adhesion, preventing rotting of the leaves. A microscopic view shows that the leaves have high roughness, trapping air bubbles in the rugosities (Figure 2.15) [8].

In biotechnology, there are cases where it is important to obtain super-hydrophobic contact. It reduces the hydrodynamic drag at the wall, and it prevents cross contamination of one drop by another one moving on the same surface. It is possible to obtain artificially superhydrophobic contact by increasing the surface roughness and mimicking the natural surface of Figure 2.15. It has been shown that a hydrophobic substrate may be rendered super-hydrophobic by etching microgrooves or micropillars [9], as shown in Figure 2.16.

Superhydrophobic surfaces are commonly microfabricated by etching micropillars in a silicon substrate. The shape of a droplet deposited on such pillars has been calculated [10] using the Evolver code [11] (see Section 2.2.7).

There are also cases where a very hydrophilic surface is suitable (e.g., to increase the wetted surface). Uelzen and Müller have shown that most solid smooth surfaces can be roughened by crystallization of pyramidal crystal of tin (Sn) of 1 to 2 μm in size [12]. Then a hydrophilic or hydrophobic layer may be deposited on top, resulting in a substantial increase in hydrophilicity or hydrophobicity. For example, the contact angle of water on gold is 80° but it drops to 60° with this technique. For

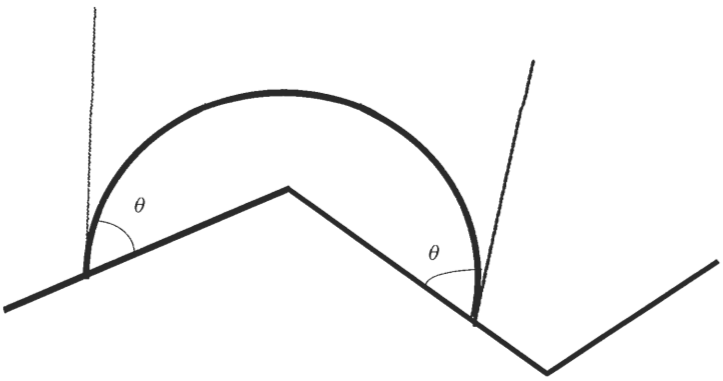

Figure 2.14 Large-scale roughness: schematic view of a drop located on an angle of the solid surface. The position of the drop might not be stable.

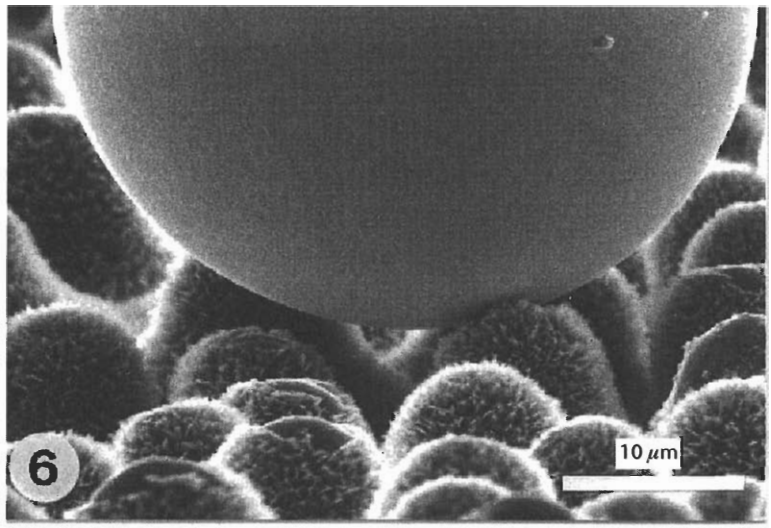

Figure 2.15 Mercury droplet on the papillose adaxial epidermal surface of Colocasia esculenta (*From:* [8]. © 1997 Planta. Reprinted with permission.)

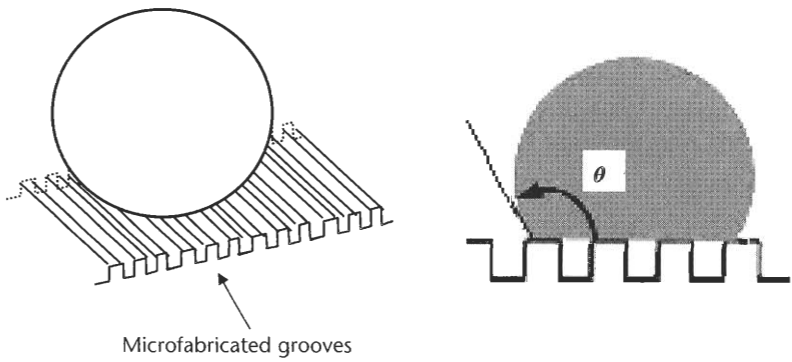

Figure 2.16 (Left) Superhydrophobic surface fabricated by etching microgrooves in a hydrophobic substrate, and (right) superhydrophobic surface constituted of micropillars.

water on hexamethyldisiloxane (HMDSO), it drops from 30° to 5°, which is a very hydrophilic contact.

2.2.5 Cassie-Baxter Law

The same analysis of Wenzel was done by Cassie for chemically inhomogeneous solid surfaces. As for Wenzel's law, the same requirement of small-size heterogeneities compared to interactions distance between liquid molecules and solid wall applies. For simplicity, we analyze the case of a solid wall constituted by microscopic inclusions of two different materials; if θ_1 and θ_2 are the contact angles for each material at a macroscopic size, and f_1 and f_2 are the surface fractions of the two materials (Figure 2.17), then the energy to move the interface of dx is

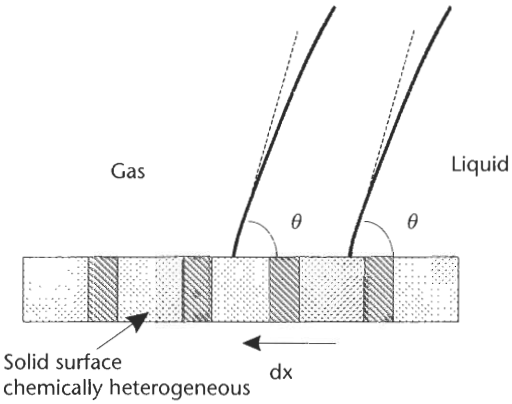

Figure 2.17 Displacement of the contact line of a drop on an inhomogeneous solid surface.

$$dE = dW = (\gamma_{SL} - \gamma_{SG})_1 f_1 dx + (\gamma_{SL} - \gamma_{SG})_2 f_2 dx + \gamma_{LG} \cos\theta dx \tag{2.15}$$

The equilibrium is obtained by taking the minimum of E

$$\gamma_{LG} \cos\theta = (\gamma_{SG} - \gamma_{SL})_1 f_1 + (\gamma_{SG} - \gamma_{SL})_2 f_2$$

and by comparing it with Young's law, we obtain the Cassie-Baxter relation

$$\cos\theta = f_1 \cos\theta_1 + f_2 \cos\theta_2 \tag{2.16}$$

This relation may be generalized to a more inhomogeneous material

$$\cos\theta = \sum_i f_i \cos\theta_i$$

Note that

$$f_1 + f_2 = 1 \quad \text{or} \quad \sum_i f_1 = 1$$

The Cassie-Baxter relation shows that the cosine of the contact angle on a microscopically inhomogeneous solid surface is the barycenter of the cosine of the contact angles on the different chemical components of the surface.

The Cassie-Baxter law explains some unexpected experimental results: Sometimes, if not enough care was taken during microfabrication, a microfabricated surface may present chemical inhomogeneity and the wetting properties are not what they were initially expected. For example, if a uniform layer of Teflon is deposited on a rough substrate, the surface should become hydrophobic. However, if the layer is too thin, the Teflon layer may be porous and the coating inhomogeneous; the wetting properties are then modified according to the Cassie-Baxter law and the gain in hydrophobicity may not be as important as expected.

As for Wenzel's law, an important remark at this stage is that the scale of change of the different chemical materials of the solid surface is *very small compared to that of the drop* [7]. Indeed, if not, it would not be possible to define a unique contact angle anymore, and the contact could be sketched as in Figure 2.18 (in such a case,

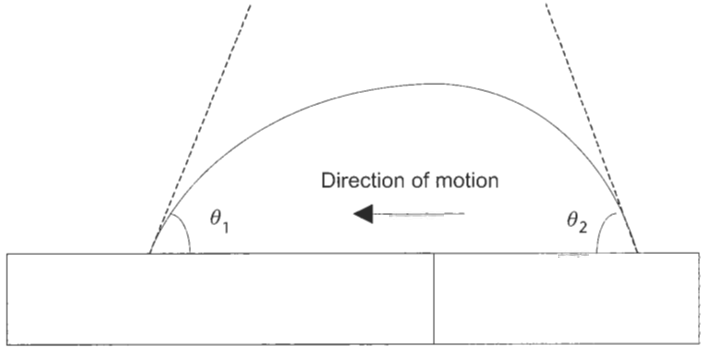

Figure 2.18 Schematic view of the contact on two different solids: the drop is not stable and migrates to the more hydrophilic surface.

we shall show later that the drop is not at equilibrium and migrates to the more hydrophilic region).

2.2.6 Simultaneous Water and Oil Superrepellent Surfaces

It is known that solid surfaces covered by fluoromethyl groups (CF_3) have very low surface energy. The contact angle with oil is 110° and with water is 95°. It is tempting to use the principles of Wenzel's and Cassie-Baxter laws to increase these contact angles and to obtain a water and oil superrepellent surface [13]. By using fractal shape surfaces, Hsieh and coworkers have obtained a rough inhomogeneous surface having contact angles larger than 150° with oil and larger than 160° with water. Note that both the Wenzel and the Cassie-Baxter laws predict the increase of contact angle values. When the roughness parameter r is increased, very small air bubbles are trapped, and the liquid droplet is partly in contact with the fluoromethyl (f_1) and partly with air (f_2). According to Wenzel's law, the contact angle increase with r, and according to the Cassie-Baxter law, it also increases because the contact angle with air is 180°. We can rewrite (2.16) under the form

$$\cos\theta = f_1 \cos\theta_1 - f_2$$

This latter relation shows an increase in contact angle as soon as air bubbles are trapped in rugosities. This shows that the problem of air trapped by very rough surfaces is still a subject of investigation.

2.2.7 The Effect of Surfactants

Surfactant is the short form for *surface active agent*. They are long molecules characterized by a hydrophilic head and a hydrophobic tail, and for this reason they are called amphiphilic molecules. More details about the chemical structure of surfactants are given in Chapter 6. Very often surfactants are added to biological samples in order to prevent the formation of aggregates and to prevent target molecules to stick to the solid walls of the microsystem (remember that microsystems have extremely large ratios between the wall surface and the liquid volume). Due to their amphiphilic nature, surfactants gather on the interface

between the liquid and the surrounding gas, as sketched in Figure 2.19(a), lowering the surface tension of the liquid [14]. Above a critical concentration, the interface is saturated with surfacatants and surfactants molecules in the bulk of the fluid group; together they form micelles.

Surface tension is reduced by the presence of surfactants at the interface, as shown in Figure 2.19(b). For example, pure water has a surface tension 72 mN/m, and water at the critical micelle concentration (CMC) has a surface tension 30 mN/m.

How is this effect of surfactants on surface tension measured? Usually one uses the pendant-drop method on small but not microscopic drops, so that the shape of the drop is a balance between surface tension and gravity forces [15]. The pendant-drop method consists of forming a drop pending from the tip of a vertical capillary tube, taking a picture of the drop, and analyzing the shape of the contour of the drop (Figure 2.20).

It can be shown that the contour is linked to the value of the surface tension. The calculation of the interfacial tension is achieved using the two following equations.

First, the Laplace equation (see Section 2.3.2):

$$\Delta P = \gamma\left(\frac{1}{R} + \frac{1}{R'}\right)$$

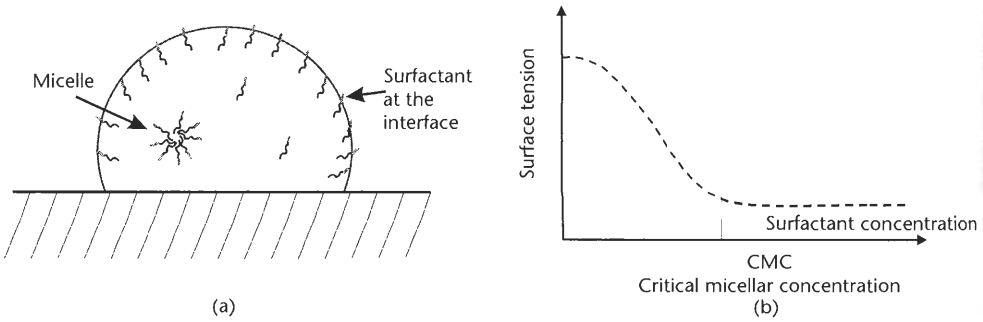

Figure 2.19 (a) Schematic view of surfactants in a liquid drop; and (b) relation between surface tension and surfactant concentration.

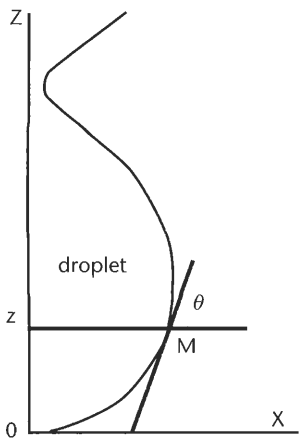

Figure 2.20 Typical drop contour in the pendant-drop method.

Second, the equilibrium equation of the drop between the interfacial tension, gravity, and pressure:

$$2\pi R\gamma \sin\theta = V(\rho_h - \rho_l)g + \pi R^2 P$$

where ΔP is the pressure difference through the interface, resulting from the curvature of the interface, R and R' are the main curvature radii of the interface, x and z are the coordinates of M on the contour of the image of the drop, θ is the angle of the tangent at M to the contour of the image of the drop, V is the volume of the fluid under the plane of altitude z, ρ_h and ρ_l are the volumic masses of the two fluids, and g is the gravitational acceleration. Substitution of the force equilibrium equation into the Laplace equation yields a relation between γ, R, R', V, and θ. The analysis of the image provides the values of R, R', V, and θ. A more precise value of the surface tension is obtained by averaging the results for many different values of z.

In the case of a liquid containing surfactants, successive pictures of the drop show an evolution of the contour related to the adsorption of surfactants on the interface [16], as shown in Figure 2.21. When CMC is reached, the shape of the drop does not change anymore.

2.2.8 Shape of a Drop on Solid Surface

We have seen in the preceding section that, in absence of other forces, the shape of a liquid drop is determined by a balance between gravitational force and surface tension. It is the same when the drop is deposited on a solid surface. It is a common observation that large drops are not spherical, but small drops are. Take a drop of water of 0.05 cm^3 volume placed on a horizontal hydrophilic plate. The real shape of the drop is shown in Figure 2.22(a); if gravitational forces are not taken into account, the shape of the drop would be spherical, as shown in Figure 2.22(b). As can be expected, the effect of gravity is to flatten the drop.

It is worth remarking that the contact angle of the liquid with the solid surface is macroscopically not the same if gravitational forces have an effect on the drop

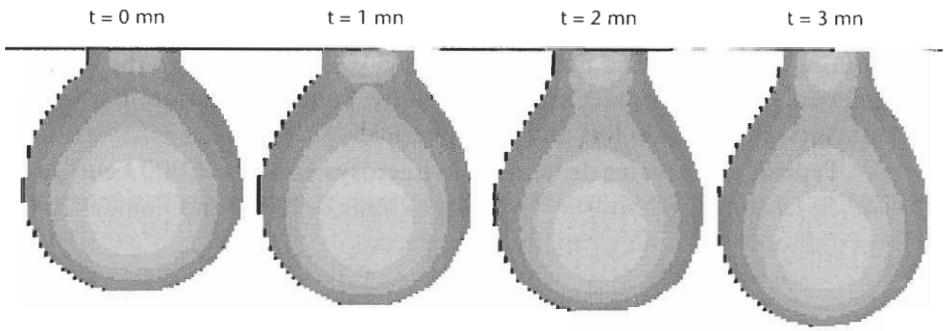

Figure 2.21 Different shapes of pendant-drop during surfactant concentration adsorption on the interface. The drop is in equilibrium between the interfacial tension and the gravity. These forces are opposed. The interfacial tension gives the drop a spherical shape, whereas the gravity elongates it. Then the drop seems to be pear shaped. The influence of the interfacial tension on the shape of the drop can be observed during the adsorption of surfactant. The drop becomes more and more elongated and the area of the interface increases when the interfacial tension decreases with time.

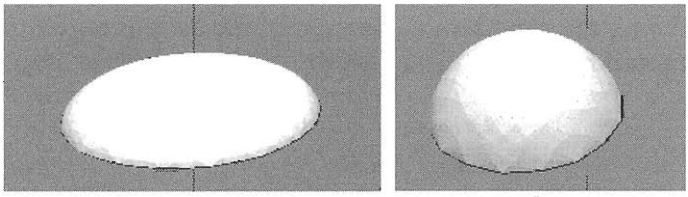

Figure 2.22 (a) The real shape, and (b) with $g = 0$ m/s^2.

shape. To this point we come back to Shapiro's energy approach [5]. Suppose a drop sufficiently small to be close to spherical, but showing a small deformation due to gravitational forces. It can be shown that the total energy of the drop (the surface energy plus the potential energy) is given by

$$E = (\gamma_{LS} - \gamma_{GS})R^2\pi\sin^2\theta + \gamma_{LG}2\pi(1-\cos\theta) + R^4\rho g\frac{2\pi}{3}(3+\cos\theta)\sin^6\left(\frac{\theta}{2}\right) \quad (2.17)$$

The two first terms in (2.17) are the surface energy (2.9), and Shapiro has shown that the third term is the potential energy. The interfacial term is at minimum when θ is equal to the nongravity contact angle, and the gravity term is at minimum when $\theta = 0$, so it tends to flatten the drop. Using the same derivation principle as before, a modified Young's equation is obtained:

$$\cos\theta - \left(\frac{\gamma_{SG} - \gamma_{SL}}{\gamma_{LG}}\right) + \left(\frac{\rho g R^2}{\gamma_{LG}}\right)\left[\frac{\cos\theta}{3} - \frac{\cos 2\theta}{12} - \frac{1}{4}\right] = 0 \quad (2.18)$$

The two first terms of this equation are just the Young's equation; the third term is a correction due to gravity. In this third term, a nondimensional number appears; that is usually called the Bond number

$$Bo = \frac{\rho g R^2}{\gamma_{LG}} \quad (2.19)$$

The Bond number represents the ratio of the gravitational forces to the surface tension. For a low Bond number, the gravity has no effect on the drop, the shape is spherical, and the contact angle is given by Young's equation. For increasing Bond numbers, the shape is less and less spherical.

Typically, for water drops used in microsystems, $\rho = 1{,}000$ kg/m^3, $\gamma = 72$ mN/m, and $R = 1$ mm at the most. This leads to a maximum Bond number of 0.15, so that gravitational force may usually be neglected.

2.3 The Physics of Drops

2.3.1 Minimization of Surface Energy

As a general rule, the equilibrium state of a physical system corresponds to a minimum of energy of the system. This rule may be applied to liquid drops. The

equilibrium shape of a drop minimizes its surface energy, taking into account all the other forces that act on the drop. This is why a drop tends to the spherical shape—when it is possible.

To show the effect of the minimization of surface energy, we give examples obtained with the public domain Surface Evolver software by Ken Brakke [11], well adapted for drops at equilibrium or near equilibrium.

Take the example of a thin liquid film on a horizontal plane, and assume that the Young's contact angle of the liquid with the solid is 80°. The results of the Evolver code are shown in Figure 2.23. The drop wants to minimize the surface energy, and it takes a spherical cap shape.

Another example is the case of a drop forming on a spherical solid sphere (Figure 2.24). We will show a very striking application of this very simple principle in Chapter 7 (dedicated to the study of magnetic beads). Actually, the liquid behavior is exactly the same as in the case of the flat plane (for sizes less than 1 μm, the gravity force does not modify the shape of the drop); just the geometry is now spherical.

2.3.2 Laplace Law

Minimization of energy also has theoretical consequences, as we are going to see with the Laplace law. The Laplace law is a relation between the pressure difference across an interface and the radius of curvature of the interface. First, for simplicity, consider a spherical drop (Figure 2.25). Assume an infinitesimal change in the radius R. The energy variation is then [3]

$$dE = -P_1 dV_1 - P_0 dV_0 + \gamma dA \tag{2.20}$$

taking into account the values of the volumes and surface

$$\begin{aligned} dV_1 &= -dV_0 = 4\pi R^2 dR \\ dA &= 8\pi R dR \end{aligned} \tag{2.21}$$

and applying the minimization theory

$$\frac{dE}{dR} = -4\pi(P_1 - P_0)R^2 + 8\pi\gamma R = 0$$

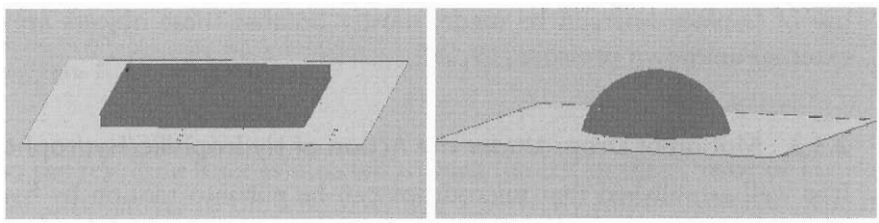

Figure 2.23 A liquid layer initially deposited on a flat solid surface is not at equilibrium; it evolves until it reaches a minimum for the surface energy. The shape of the drop is then a spherical cap. The first (left) view is not physical; the final (evolved) shape is the equilibrium shape.

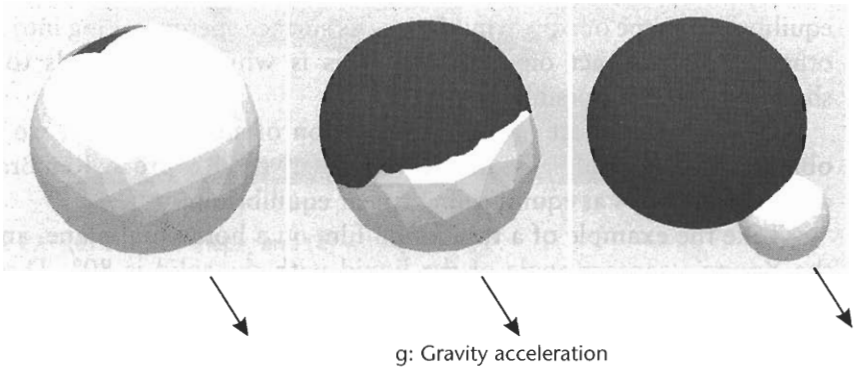

Figure 2.24 A liquid layer initially covers nearly entirely a solid sphere (far left), but due to the constraint of a 120° contact angle, the layer "peels off" and forms a spherical cap attached to the solid sphere.

and we find the Laplace equation for spherical drops

$$P_1 - P_0 = 2\frac{\gamma}{R} \tag{2.22}$$

Note that in the general case, there are two radiuses of curvature at the drop surface R and R'. In this case, the derivation of the Laplace law requires more algebra. We just indicate the result

$$P_1 - P_0 = \gamma\left(\frac{1}{R} + \frac{1}{R'}\right) \tag{2.23}$$

Laplace law signifies that there is a discontinuity in pressure when crossing an interface. The result may seem simple, but it hides some complications: first note that the pressure inside a microdrop equilibrates very quickly because of the size of the drop. So what to think of drops for which curvature radius is not constant? Take the example of Figure 2.25 (right part). There is a change of curvature radius when the bubbles are facing each other. Because the inner pressure is uniform, Laplace law indicates that the pressure in the liquid film between the two bubbles P_i is larger than the pressure P_0.

The use of Laplace law is often a very elegant way to solve drop deformation [17, 18], and it has been thought to apply this law to in-vivo situations, like for the lung alveoli or vesicles. But in these two latter cases, it has been shown that incorrect use of Laplace law can be made, mostly because these objects are deformed by external unknown pressure [19, 20].

2.3.3 Motion of Drops Under the Action of Hydrophilic/Hydrophobic Forces

It is well established that microdrops can be put into motion by hydrophilic and hydrophobic forces. Let's suppose for an instant that a water droplet is placed on a perfectly smooth horizontal plane (Figure 2.26) at the boundary between two different chemical coatings: hydrophilic on one side and hydrophobic on the other

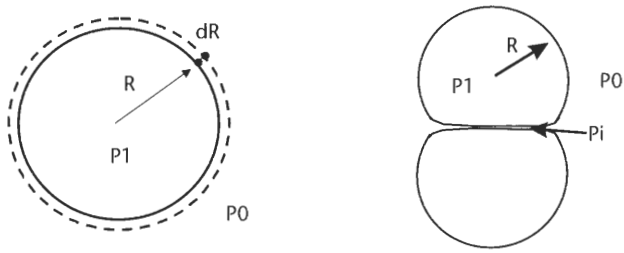

Figure 2.25 Scheme of a spherical drop and an elementary change in radius (left), and schematic view of two bubbles in a foam (right).

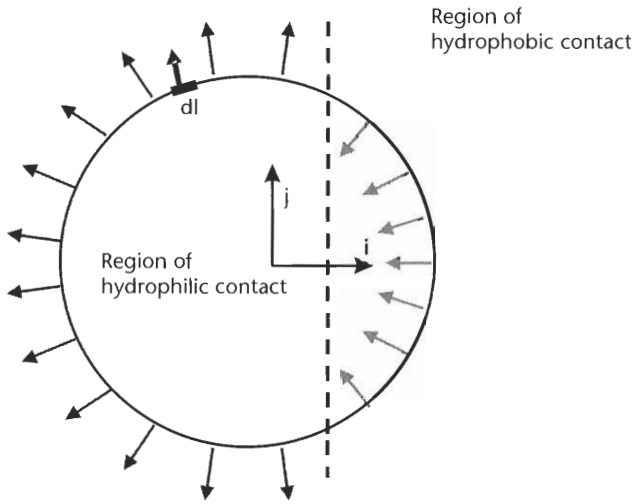

Figure 2.26 Schematic view of a water droplet standing above a hydrophilic/hydrophobic contact. There is a resulting force directed toward the hydrophilic region.

one. In such a case, this scheme can be used for the contact forces (as we do not know the exact shape of the drop at the very instant it is placed on the surface, we have drawn an approximate shape, close to—but not exactly—a circle; however, the reasoning will stand, whatever the shape).

From this scheme, it results that the droplet is displaced toward the hydrophilic surface. If L_1 and L_2 are the contact lines, respectively, in the hydrophilic and hydrophobic plane, and θ_1 and θ_2 are the contact angles, the force acting on the drop is

$$F_x \int_{L_1} = (\gamma_{SG} - \gamma_{SL})_1 \left(\vec{i} \cdot d\vec{l}\right) + \int_{L_2} (\gamma_{SG} - \gamma_{SL})_2 \left(\vec{i} \cdot d\vec{l}\right) = \int_{L_1} \gamma_{LG} \cos\theta_1 \left(\vec{i} \cdot d\vec{l}\right) + \int_{L_2} \gamma_{LG} \cos\theta_2 \left(\vec{i} \cdot d\vec{l}\right) < 0 \tag{2.24}$$

So the resulting force is directed toward the left in the scheme of Figure 2.26, and the drop moves to the left (assuming a perfectly smooth surface). The motion stops when the resultant of the contact forces is zero (i.e., when the drop is entirely on the hydrophilic region, as shown in Figure 2.27). It would be the same if there were wettability gradient [21].

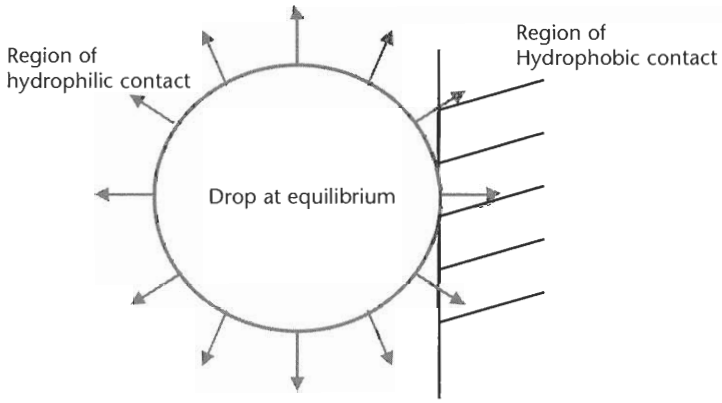

Figure 2.27 The drop is at equilibrium when it is entirely located on the hydrophilic region.

Experimental evidence confirms the preceding analysis: In Figure 2.28, a drop is deposited with a micropipette on a flat horizontal surface at the boundary of two regions with different contact angles.

The preceding analysis is also confirmed by a calculation with the Evolver code (Figure 2.29). We can start with any unphysical volume of liquid spread over a hydrophilic/hydrophobic boundary. After a few iterations, the drop is formed, but it is not at equilibrium because of the global force directed toward the hydrophilic region. The drop evolves to find its equilibrium location, which is located just at the boundary of the transition line but on the hydrophilic side.

Note that the direction of the motion of a water drop is toward the hydrophilic region, whereas the motion of an oil droplet would be toward the hydrophobic region in the same geometrical conditions.

Another striking example of capillary forces is that they can be sufficient to make drops move upward. Chaudhury and coworkers [22] have shown that a drop can go up a slightly inclined plate, presenting a wettability gradient as shown in Figure 2.30.

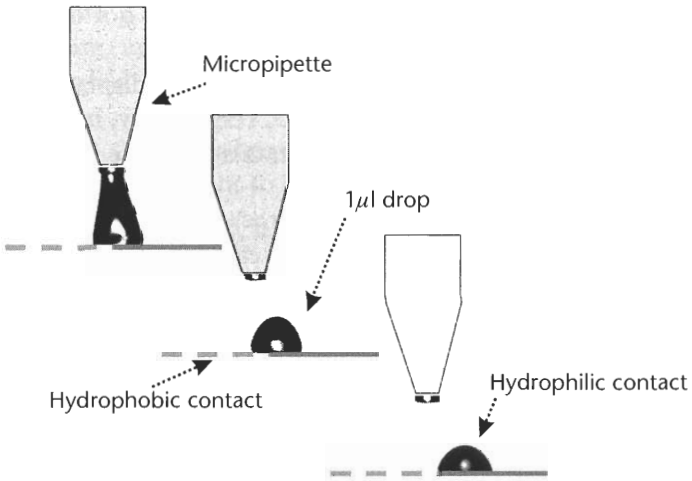

Figure 2.28 Experimental view of the relocation of a microdrop (1 μl) deposited on a hydrophilic/hydrophobic boundary.

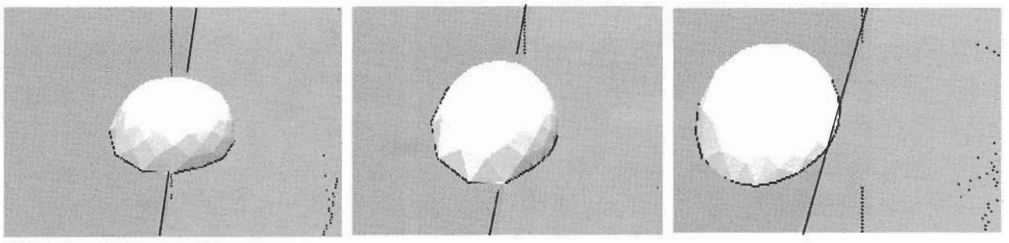

Figure 2.29 Motion of a drop toward the hydrophilic plane (simulation with Surface Evolver). The microdrop is initially deposited over the hydrophilic/hydrophobic transition line, and it is not an equilibrium state. Drop moves to find an equilibrium state on the hydrophilic plate, just at the boundary between the two regions.

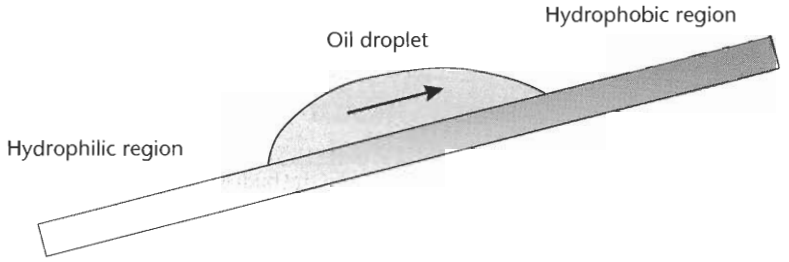

Figure 2.30 An oil drop may run uphill toward the more hydrophobic region.

Another interesting demonstration of the power of capillary forces—occurring in microsystems—may be shown by making a drop move up a step: in such a case, a microdrop is initially located on a step at the boundary of a hydrophilic region (on top of the step) and a hydrophobic region (at the base of the step). The calculation with the Evolver code shows that the drop progressively moves toward the hydrophilic region, even if this region is located at a higher level (Figure 2.31). Capillary forces dominating gravity is this example.

Note that in this section, we have considered the surface perfectly smooth, and we have neglected the effect of hysteresis. In reality, a drop does not move as soon as there is a gradient of wettability. The drop moves as soon as the gradient of wettability is sufficient for the capillary forces to dominate the hysteresis reaction force.

2.3.4 Marangoni Effect

As a general rule, surface tension is not constant; it depends on temperature and concentration of chemical species at the surface. The classical relation between surface tension and temperature is [23]:

$$\gamma = \gamma_0\left(1-\beta(T-T_0)\right) \tag{2.25}$$

This is a first-order relation, but it is sufficient to describe the variation of surface tension with temperature. For an interface water/air, $\gamma_0 = 72$ mN/m and (β γ_0) ~ 0.1 mN/m. This change of surface tension with temperature has important consequences in microphysics of drops. The most common example is that of

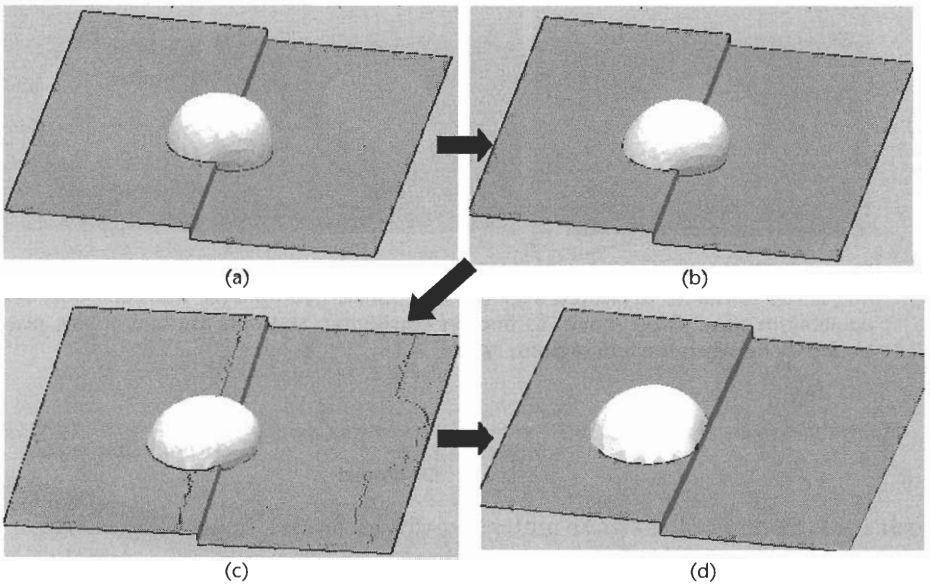

Figure 2.31 Motion of a drop up a step toward the hydrophilic plane (simulation made with Surface Evolver): (a) the drop is deposed on the step; (b) as (a) is not an equilibrium state, the drop moves up the step pulled by the hydrophobic forces of the upper plate and pushed by the hydrophobic forces of the lower plate; (c) motion continues; and (d) equilibrium state is reached when the drop is entirely on the upper plate.

Marangoni convection—also called thermocapillarity or surface tension–induced convection [23]. Each time a drop is not isothermal, there is a gradient of temperature at the interface and subsequently, due to (2.25), a gradient of surface tension. Reminding that surface tension can be looked at as a force, the surface tension distribution at the liquid/gas interface induces a tangential force distribution on the interface. These tangential forces act as a motor at the fluid interface and may lead to a convective motion inside the drop (Figure 2.32). This phenomenon is very common in microfluidics and is called Marangoni convection.

A classical example is that of a drop maintained between a solid surface and the tip of a needle. If the solid surface is maintained at a temperature T_1, and the tip of the needle is at a temperature T_2, then a convective motion appears in the drop, as schematized in Figure 2.33.

The intensity of the Marangoni convection is linked to a nondimensional number, the Marangoni number Ma defined by

$$Ma = \frac{\Delta\gamma R}{\rho\nu\alpha} \tag{2.26}$$

where $\Delta\gamma$ is the variation of the surface tension, R is the radius of the drop, ρ is the density of the liquid, ν is the kinematic viscosity, and α is the thermal diffusivity.

Another example of the Marangoni effect is found in microwells of DNA arrays. DNA arrays are designed for the recognition of DNA segments. The principle is quite simple: it is based on the matching between a target DNA and its complementary sequence. When the target DNA finds its complementary sequence,

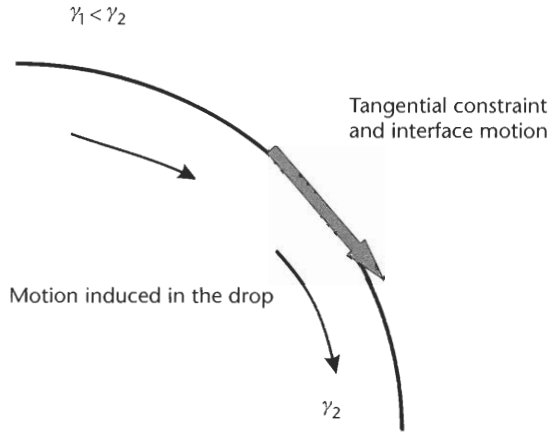

Figure 2.32 Surface tension gradient exerts a tangential constraint on the interface, resulting in a tangential motion. Viscosity diffuses the motion inside the droplet. This phenomenon is called Marangoni convection.

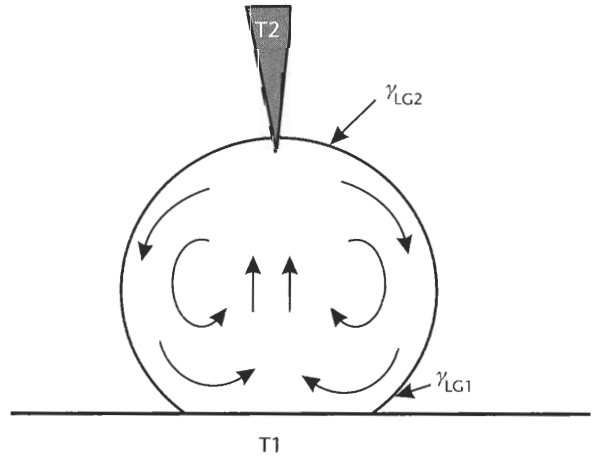

Figure 2.33 Schematic view of a Marangoni-driven convection inside a droplet. Here $T_1 < T_2$ and the surface tension γ_{LG1} is larger than γ_{LG2}, so that the convective motion on the surface is directed from the needle tip to the solid plate.

there is a binding between the two segments due to hydrogen bonds. Because we don't know the target—suppose it is the DNA of some virus that we want to identify—we use a microplate with many microwells or cusps. Each well is grafted with a predetermined DNA sequence so that each well aims at a specific target. The target can be identified by fluorescence when it binds in a well. Grafting of complementary sequences in the bottom of a cusp requires successive operations of deposition of liquid drops and heating for evaporation. As the heating of the drop is not uniform, surface tension is lower at the walls, and the liquid rises along the walls due to increased capillarity (Figure 2.34). Cusps should then be designed in a way that the liquid cannot exit by capillarity and overflow in the neighboring cusps.

Another type of Marangoni convection may occur in biological microsystems due to surfactants concentration. Figure 2.35 shows the well-known picture of a

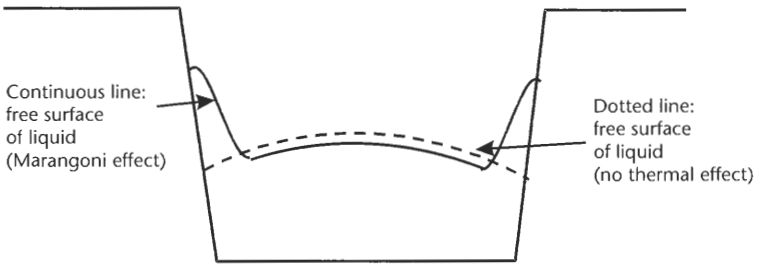

Figure 2.34 The Marangoni effect in a microwell of a DNA array. Note that in the case of a uniform temperature, the surface tension is constant, and the interface is a spherical cap with the usual contact angles, whereas in the case where the drop is heated, the interface is deformed by the Marangoni effect.

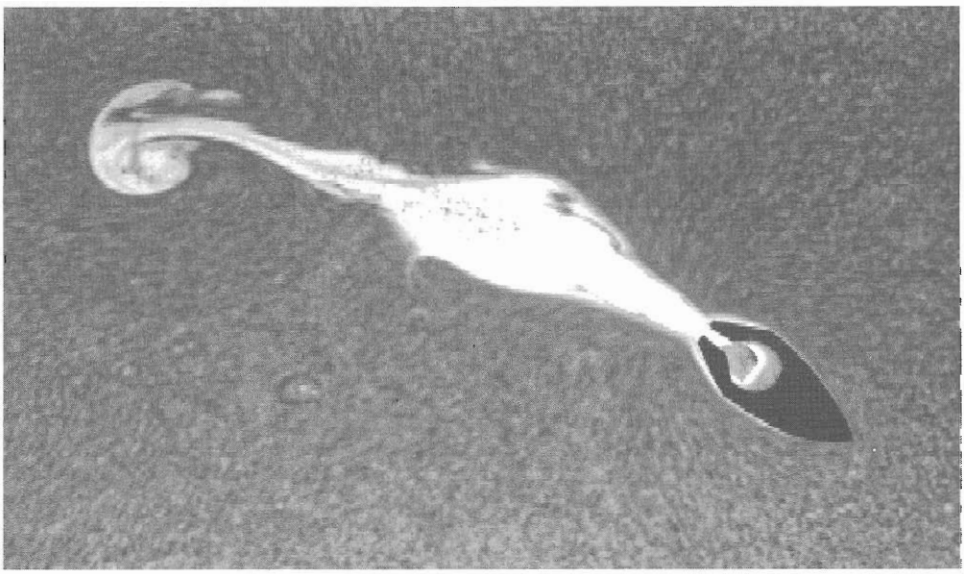

Figure 2.35 The soap boat: A floating body contains a small volume of soap; the soap exits the rear of the boat, decreasing locally the surface tension. The resulting gradient of surface tension at the surface of the liquid makes the water move toward the high surface tension region, and this motion of the water propels the boat [24]. (Courtesy of John Bush, David Hu, and Brian Chan, Department of Mathematics, MIT.)

soap boat: a floating body releases soap at the surface of water, creating a gradient of surface tension; water moves from low surface tension regions to high surface tension regions to equilibrate the surface tension; consequently the boat moves forward, toward the high surface tension region.

We have already seen that the surface tension changes with surface concentration of surfactants [25]. When surfactants are added to the biofluid, they migrate to the interface, and a gradient of interface concentration may occur, leading to a convective motion of the interface (Figure 2.36).

In the case of concentration-induced Marangoni convection, it is possible to define a nondimensional Marangoni number by

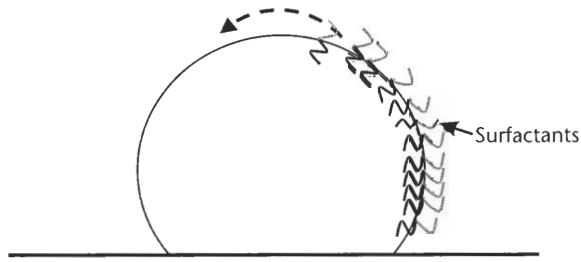

Figure 2.36 Surfactants migrate on the surface in order to homogenize their surface concentration.

$$Ma = \frac{\Delta\gamma R}{\rho\nu D} \tag{2.27}$$

where D is the diffusion coefficient.

In a more general approach, it can be shown that Marangoni convection can have three different causes: thermal gradient, concentration gradient, and electrical gradient [26]. If we write the surface tension under the form

$$\gamma = \gamma(T, c, V)$$

where T is the temperature, c is the concentration, and V is the electric potential, then

$$\nabla\gamma = \frac{\partial\gamma}{\partial T}\nabla T + \frac{\partial\gamma}{\partial c}\nabla c + \frac{\partial\gamma}{\partial V}\nabla V$$

2.3.5 Microdrops Evaporation

Microdrops have surface-to-volume ratios much larger than usual macroscopic drops. For a spherical drop, the surface-to-volume ratio is

$$\frac{S}{V} = \frac{3}{R} \tag{2.28}$$

and, for a spherical drop placed on a solid horizontal surface, using relation (2.3) and (2.8)

$$\frac{S}{V} = \frac{3}{R}\frac{2}{\left(2 - \cos\theta - \cos^2\theta\right)} \tag{2.29}$$

It can be easily shown that for any contact angle θ, the ratio S/V is larger than

$$\frac{S}{V} \geq \frac{8}{3R} \tag{2.30}$$

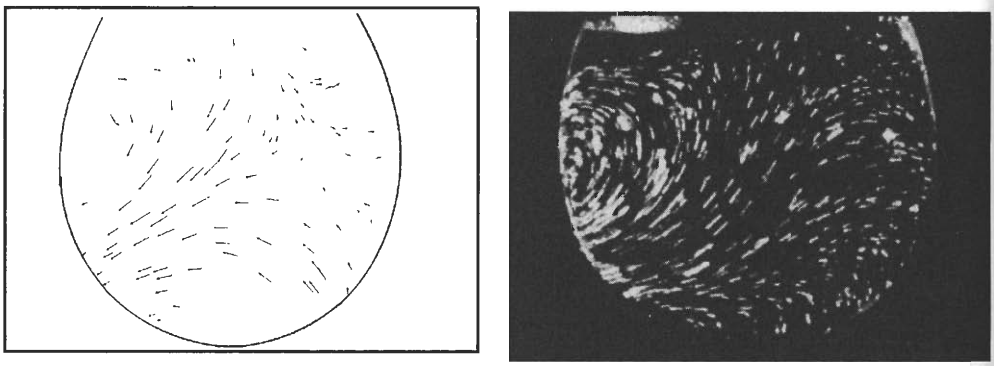

Figure 2.37 Marangoni convective motion due to evaporation in a water droplet. (*From:* [27]. © 1996 American Physical Society. Reprinted with permission.)

This relation shows that microdrops have a large surface-to-volume ratio, and they rapidly tend to evaporate in an open environment. It is important when working with droplets to estimate the lifetime of a droplet. The classical Maxwell model for a drop lifetime assumes that the evaporation process is controlled by a mass diffusion process exterior to the droplet and leads to a total lifetime

$$\tau = \frac{R_0^2 \rho}{2D\Delta c} \tag{2.31}$$

where R_0 is the initial radius, ρ is the density of the evaporating media, and Δc is the concentration change from droplet surface to ambient concentration (far from droplet).

However, it was shown [27] that this lifetime is largely overestimated, because it does not take into account convective motion inside the droplet. It is established that this convective motion is due to a Marangoni effect. The evaporation process induces a heat flux at the drop surface and consequently a temperature gradient inside the drop. This conductive state usually becomes unstable: Imagine a very small area at the surface where the evaporation rate is stronger than the average; the local temperature is then smaller than average surface temperature, resulting in a surface tension gradient. This surface tension gradient leads to a Marangoni-type convection (Figure 2.37). This convective motion may be very strong (velocities of 1 mm/sec in a 2-mm diameter drop for $\Delta T = 1°C$) and has a random behavior because the location of the "cold spot" on the surface changes randomly.

Finally the convection inside the drop causes a much stronger evaporation rate than that predicted by the conductive Maxwell model. A water drop with an initial radius of 200 μm and a $\Delta T = 1°C$ will evaporate in 5 minutes (instead of a value of more than 10 hours predicted by the conductive theory). An approximated lifetime was derived by Hegseth and coworkers based on the Marangoni number and the Jacob number

$$\tau \approx \frac{R_0^2}{\alpha Ja} \frac{1}{(1+Ma)} \tag{2.32}$$

where α is the thermal diffusivity of the liquid, and Ja is the Jacob number given by

$$Ja = \frac{C_P \Delta T}{h_{LG}} \tag{2.33}$$

Ja is nondimensional; it is the ratio between the conducted heat and the latent heat of vaporization (per unit mass). The lifetime of a droplet is largely overestimated by the formula in (2.31), based on a diffusion-only process. In reality, the Marangoni convection, due to spatial instabilities of evaporation rates, leads to a much shorter lifetime of the droplet, as expressed by (2.32).

The preceding paragraph dealt with spherical or nearly spherical drops (wetting angle sufficiently important). For drops having a small contact angle on a solid surface, evaporation takes another aspect. Very often, one observes a ring when the drop has completely dried, as shown in Figure 2.38 [28]. The reason is that evaporation is stronger at the boundary of the drop, and a convective motion carries particles from the center to the periphery; these particles are then deposited as a ring on the initial periphery of the drop.

In conclusion, evaporation is always a concern when working with microdrops. Most of the time in biotechnology, biologic liquids have a water base, and there are some means to limit evaporation. One of them is to maintain a controlled environment with a partial pressure of vapor; another is to include the microdrops in an organic nonmiscible layer, like oil, or to add glycerol to the solution when it is chemically acceptable. Finally, as we will see in the next section, drops may be maintained between two parallel plates, and their contact surface with air is largely reduced (Figure 2.39).

2.4 The Example of Electrowetting

We have so far analyzed the behavior of drops; in this section, we give an example of microsystems using drop microfluidics.

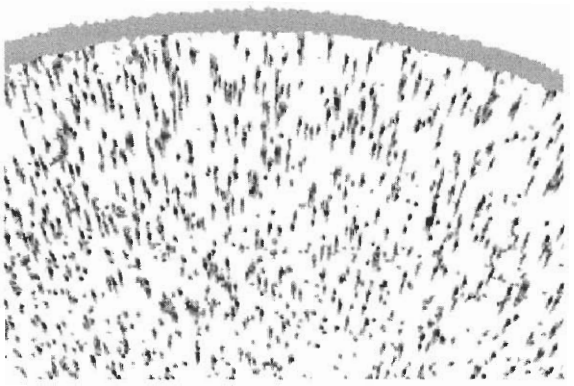

Figure 2.38 Circular ring left by an evaporating droplet. (*From:* [28]. © 2000 American Physical Society. Reprinted with permission.)

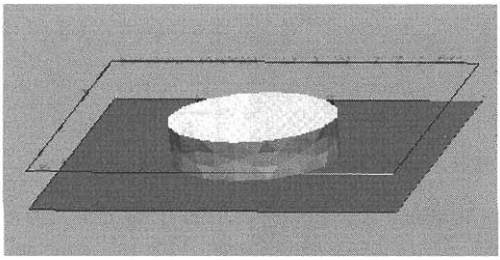

Figure 2.39 Drop confined between two parallel plates (calculation by Surface Evolver); the upper plate has been dematerialized for visualization.

In the preceding paragraphs we saw that the shape of a liquid drop on a surface is determined by the nature of the liquid, by the nature and morphology of the underlying solid, and by the surrounding fluid. It has been observed that when an electrical potential is applied, ions and dipoles redistribute in the liquid and to a lesser extent in the solid. This redistribution can cause a change in the wetting properties of the drop, according to Lippmann's law [29]. A hydrophobic surface (like Teflon) can behave like a hydrophilic surface when an electric potential is actuated: this phenomenon is called electrowetting. It is then possible to use time-regulated electric potential to displace, merge, and divide drops to perform biologic operations [30–34].

2.4.1 Principle and Theory

Lippmann's law states that the surface tension γ_{SL} of an electrically conductive liquid (surface tension between the liquid and the substrate) changes when the drop is placed in an electric field. Electric charges migrate to the liquid/substrate interface and consequently toward the contact angle. Lippmann's law can be expressed by the relation

$$\gamma_{SL} = \gamma_{SL,0} + \frac{1}{2} CV^2 \tag{2.34}$$

where C is the capacitance of the material layers in the substrate, V is the electric potential, and the index 0 refers to the nonactuated state. Combining Lippmann's law with Young's law, we obtain the well-known Lippmann-Young relation established first by Berge [35]

$$\cos\theta = \cos\theta_0 + \frac{1}{2}\frac{C}{\gamma_{LG}} V^2 \tag{2.35}$$

showing that the contact angle of a drop on a substrate can be changed by applying an electric field. Relation (2.35) has been experimentally verified on a device of the type sketched in Figure 2.40. Experimental observations of electrowetting effect are shown in the Figure 2.41.

With this in mind, drop displacement can be achieved by a difference in the electric field between two opposite sides of a drop, produced by actuated and nonactuated electrodes embedded in a solid, hydrophobic, and electrically

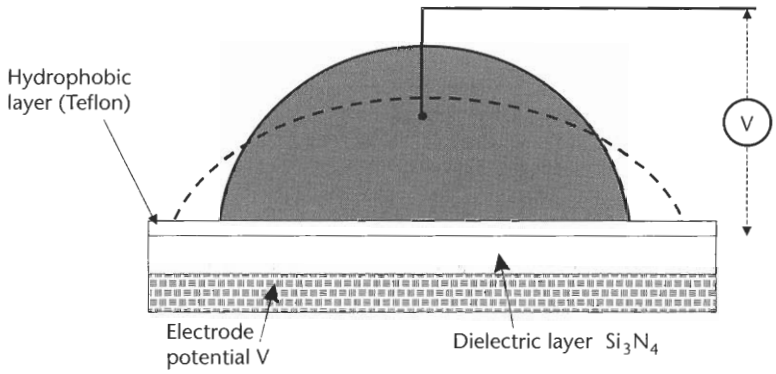

Figure 2.40 Principle of electrowetting on dielectric (EWOD): The wetting angle decreases when the drop is placed in an electrical field (dc or ac). Electric charges appear in the liquid at the contact of the substrate, and the contact angle changes.

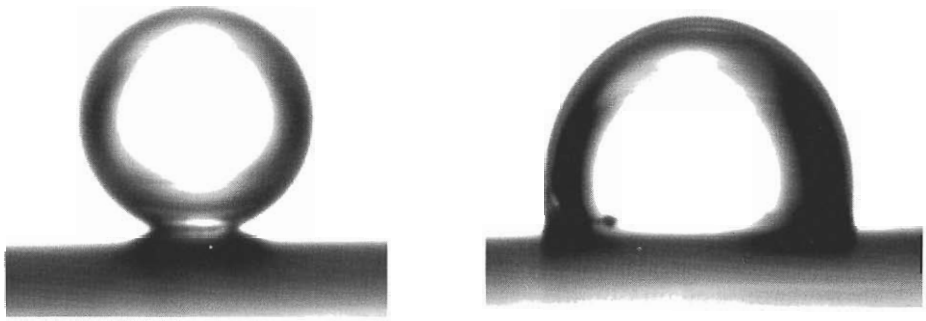

Figure 2.41 Microdrop on a hydrophobic substrate (left), and change of contact angle after actuation of an electric field (right).

insulating substrate (Figure 2.42). The contact angle is then different on the two opposite sides of the drop. A gradient of wettability is then created between two opposite sides of the droplet. Assuming there is no hysteresis (i.e., the surface is perfectly smooth) the drop moves in the direction of the smaller contact angle.

The Lippmann-Young equation can be derived by an energy minimization approach [5]. The total energy of the drop submitted to an electrical field is the sum of the surface energy and the electric potential energy

$$E = R^2\left[\left(\gamma_{LS} - \gamma_{GS} - \frac{CV^2}{2}\right)\pi \sin^2\theta + \gamma_{LG}\, 2\pi(1-\cos\theta)\right] \tag{2.36}$$

In (2.36), the right-hand side is the sum of the interfacial energy from (2.9) and a term corresponding to the electric energy. It can be shown [5] that minimization of the total energy E leads to

$$\cos\theta - \left(\frac{\gamma_{LS} - \gamma_{GS}}{\gamma_{LG}} + \frac{CV^2}{2\gamma_{LG}}\right) = 0 \tag{2.37}$$

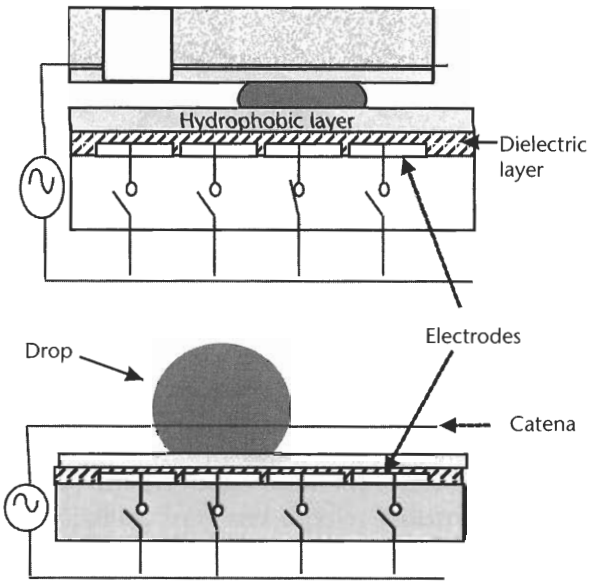

Figure 2.42 Top: "closed" or "covered" EWOD system; the drop is squashed between two horizontal parallel plates. The upper plate is at zero potential, whereas the potential of the lower plate may be adjusted. Bottom: "open" EWOD system. A catena is used to fix the zero potential. (*From:* [39]. © 2005 NSTI. Reprinted with permission.)

This equation is identical to Lippmann-Young equation (2.35), showing that the drop shape is again obtained by energy minimization.

Figure 2.43 shows a comparison between the theoretical Lippmann-Young equation and measurements. The results agree at first, for small values of the potential, but show a saturation limit not predicted by the theory (Figure 2.44). This saturation limit is currently the object of many investigations, and different explanations have been proposed [36–38]. For the rest of this section, it is worth

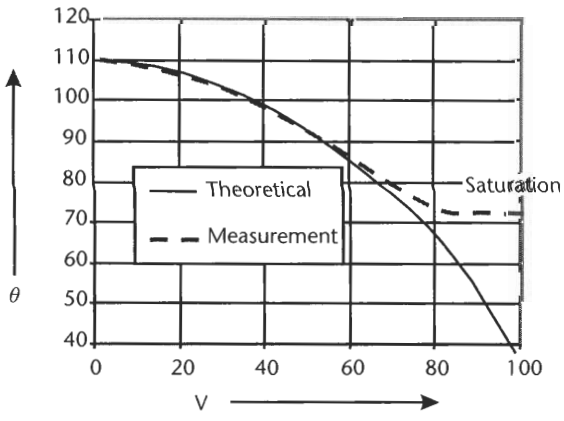

Figure 2.43 Contact angle versus electric potential: continuous line corresponding to the Lippmann-Young equation, and dotted line corresponding to the experimental results. Saturation occurs above a value of the electric potential, and the contact angle cannot be reduced further by increasing the difference of potential.

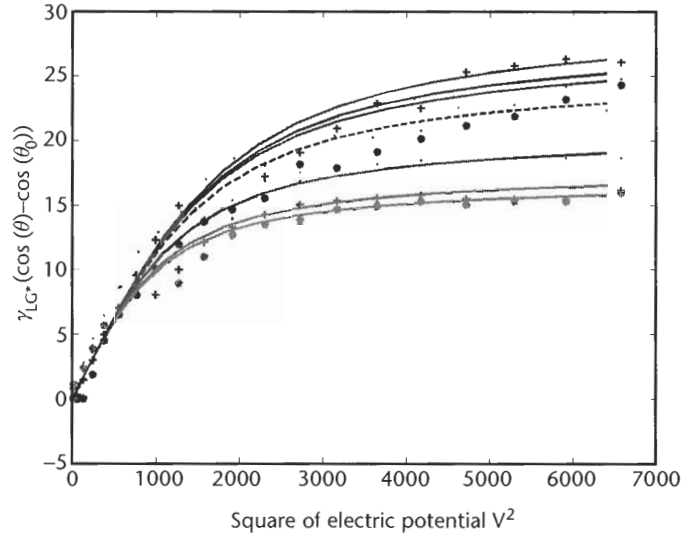

Figure 2.44 Saturation of the electrowetting effect: according to Lippmann's law (2.34) a plot of $\gamma \cos\theta - \gamma \cos\theta_0$ versus V^2, the plot should be a linear curve. This is the case for low potentials but not for large potentials.

remembering that above a certain value of the potential, the contact angle does not decrease any more.

EWOD microdevices are aimed at performing manipulations on microdrops. Figure 2.45 shows an electrode cross where a microdrop can be moved anywhere on the cross.

Among the different EWOD systems, the "covered" system appears to be more workable. In such systems, the drop is confined between two parallel horizontal plates, as shown in Figures 2.42 (top) and 2.46.

It can be shown that this is the solution requiring the less energy and for which the different operations of dispensing, dividing, and merging drops are the easiest [39].

2.4.2 Modeling Electrowetting

Different approaches to the modeling of electrowetting are found in the literature, most of which involve the dynamic approach using the Navier-Stokes equations, incorporating Young's constraint, and a volume of fluid (VOF) numerical formulation [40, 41]. However, inertia and viscous forces can often be neglected in front of surface tension.

Suppose a sessile drop of water placed on an electrode row. The surface energy of the drop is given by

$$E_S = \gamma S = \gamma 2\pi R^2 (1 - \cos\theta)$$

where R is the radius of the sphere (curvature), and θ is the contact angle. On the other hand, the kinetic energy is given by

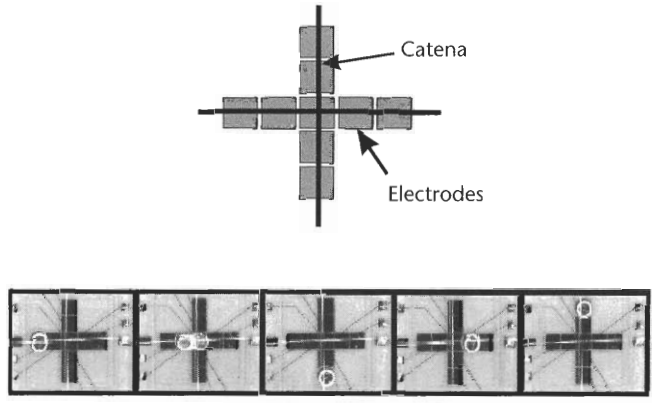

Figure 2.45 The electrode cross is constituted of nine electrodes. By switching on one electrode at a time, the drop moves and can be addressed anywhere in the cross. (Courtesy of CEA/LETI.)

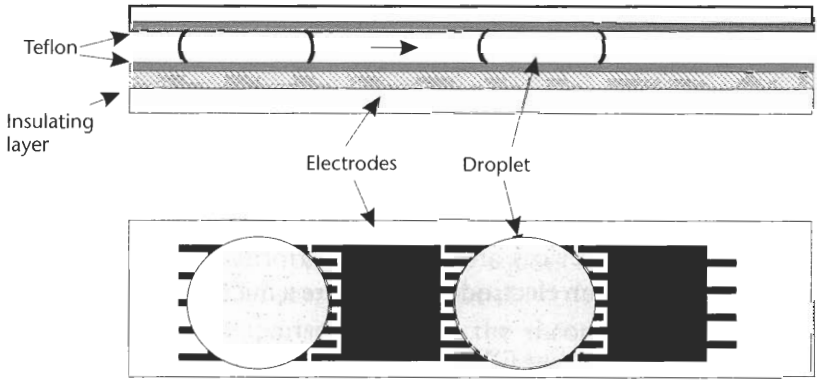

Figure 2.46 (Top) Side view of a covered EWOD device; and (bottom) top view of an electrodes' alignment.

$$E_K = \frac{1}{2}mv^2 = \frac{1}{2}\rho V v^2 = \frac{1}{2}\rho \frac{\pi R^3\left(2-3\cos\theta+\cos^3\theta\right)}{3}v^2 \tag{2.38}$$

where v is the velocity of displacement of the drop between two electrodes. The ratio between these two energies is

$$W_{EM} = \frac{E_K}{E_S} = \frac{\rho R\left(2-3\cos\theta+\cos^3\theta\right)v^2}{12\gamma(1-\cos\theta)} = \frac{\rho R v^2}{\gamma}g(\theta) \tag{2.39}$$

where

$$g(\theta) = \frac{\left(2-3\cos\theta+\cos^3\theta\right)}{12(1-\cos\theta)} = \frac{2-\cos\theta-\cos^2\theta}{12}$$

We note immediately that the nondimensional W_{EM} number is very similar to the nondimensional Weber number for a spherical drop of diameter D, given by

$$We = \frac{\rho D v^2}{\gamma} \tag{2.40}$$

We can look at W_{EM} as a "modified" Weber number. Note that the Weber number is used to describe the behavior of a jet of drops (like ink jet printers); it characterizes the ratio between inertia and surface tension and—together with the Reynolds number—governs the "splash" of the drop on the solid surface.

Suppose now that $\theta = 90°$, then $W_{EM} = \frac{\rho R v^2}{6\gamma}$. Typical displacement velocities in EWOD electrowetting are approximately of the order of 1,000 μm in 0.1 second (i.e., 0.01 m/s). For a water drop in contact with air, a typical value is $W_{EM} \approx \frac{R}{4.3}$. Thus, a 1-mm radius drop has Weber number of about 1/4,000. This shows that in most cases, the surface tension is what governs the physics of the displacement of drops in EWOD processes.

It can be shown that viscosity effects can also be negated by calculating the ratio between viscous forces and capillary forces given by the nondimensional Ohnesorge number

$$On = \frac{\mu}{\sqrt{\rho l \gamma}} \tag{2.41}$$

where l is a typical length for the drop; usually $l = R$.

Typically the Ohnesorge number is less than 0.025, which is lower than the critical value of 0.1 [42].

These results have an important consequence. It leads us to understand that the behavior of drops in electrowetting devices is mostly a morphological problem. The behavior of drops in EWOD microsystems is dominated by surface tension forces and Young's constraints at the apparent contact of the solid walls. The problem is mostly topological with the drop shape and behavior adapting to the morphology of the electrodes. Minimization of drop surface energy is a well-adapted method to solve such problems. With this approach, a quasi-steady state model using the Evolver numerical software [11] is adequate to predict drop behavior [39].

Figures 2.47 and 2.48 show the results of the modeling of drop division (splitting in two) and drop dispense (extraction from a reservoir) compared to experimental results.

2.5 Conclusion

Microdrops are an unavoidable feature in biotechnology, and it seems that microarrays using microdrops fluidics are gaining importance, especially for DNA analysis and cells manipulation. In this chapter, we analyzed the physics of liquid/solid contact and exposed some of the behaviors of microdrops. Understanding the mechanical behavior of drops is not an easy task, and we dealt with only some elements of the problem—our concern was mostly static or quasi-static aspects occurring when using microplates and electrowetting.

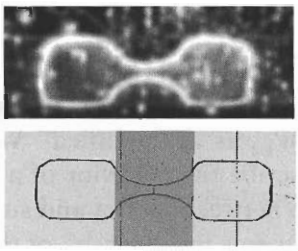

Figure 2.47 Drop division: a comparison between experimental results (top) and numerical results (bottom). Drop division is obtained by a combined effect of stretching by hydrophilic forces acting on two opposite sides of the drop (electrode actuated) and pinching in the center by hydrophobic forces (electrode not actuated). (Courtesy of D. Jary, CEA/LETI.)

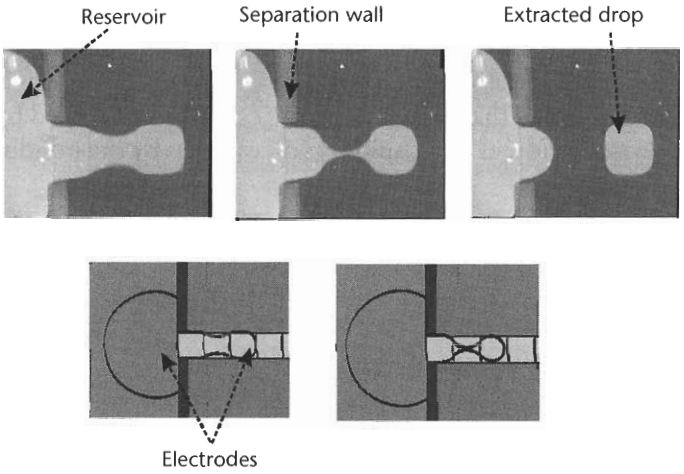

Figure 2.48 Formation of microdrops by electrowetting (drop dispense from a reservoir): experimental view (top), and numerical results (bottom). Note that the microdrop tends to mimic the form of the square electrode. Extraction is a difficult operation [17] and requires at the same time stretching by hydrophilic forces applied on the right side of the drop, pinching by hydrophilic forces at the "pinching" electrode, and back pumping from the reservoir (reservoir electrode actuated). (*From:* [39]. © 2005 NSTI. Reprinted and revised with permission.)

The first two chapters dealt with microfluidics in its two forms—microflows and microdrops—in order to predict the behavior of the carrier fluid; in the next two chapters, we present the microparticles that are convected by—or diffusing in—the carrier biofluid.

References

[1] Israelachvili, J., *Intermolecular and Surface Forces*, New York: Academic Press, 1992.

[2] de Gennes, P. G., F. Brochard-Wuart, and D. Quéré, *Gouttes, Bulles, Perles et Ondes*, Paris: Belin, 2002, pp. 13–14.

[3] Table of surface tension: http://www.gewater.com/library/tp/772_Hydrophilicity_and.jsp.

[4] Table of surface tension for chemical fluids: http://www.surface-tension.de.

[5] Shapiro, B., et al., "Equilibrium Behavior of Sessile Drops Under Surface Tension, Applied External Fields, and Material Variations," *J. Applied Physics*, Vol. 93, No. 9, 2003, pp. 5794–5811.

[6] Spherical cap volume and surface: http://mathworld.wolfram.com/SphericalCap.html.

[7] Wolansky, G., and A. Marmur, "Apparent Contact Angle on Rough Surfaces: The Wenzel Equation Revisited," *Colloids and Surfaces A: Physicochemical and Engineering Aspects*, Vol. 156, 1999, pp. 381–388.

[8] Barthlott, W., and C. Neinhuis, "Purity of the Sacred Lotus, or Escape from Contamination in Biological Surfaces," *Planta,* Vol. 202, 1997, pp. 1–8.

[9] Callies, M., et al., "Microfabricated Textured Surfaces for Super-Hydrophobicity Investigations," *Microelectronic Engineering*, Vol. 78–79, 2005, pp. 100–105.

[10] Patankar, N. A., and Y. Chen, "Numerical Simulation of Droplet Shapes on Rough Surfaces," *Proc. 2002 Nanotech Conference*, Puerto-Rico, April 21–25, 2002, pp. 116–119.

[11] Brakke, K., "The Surface Evolver," *Exp. Math.*, Vol. 1, 1992, p. 141.

[12] Uelzen, T., and J. Müller, "Wettability Enhancement by Rough Surfaces Generated by Thin Film Technology," *Thin Solid Films*, Vol. 434, 2003, pp. 311–315.

[13] Hsieh, C. -T., et al., "Influence of Surface Roughness on Water and Oil Repellent Surfaces Coated with Nanoparticles," *Applied Surface Science*, Vol. 240, 2005, pp. 318–326.

[14] Hiemenz, P., and R. Rajagopalan, *Principles of Colloid and Surface Chemistry*, New York: Marcel Dekker, 1997.

[15] Drop tensiometer and interface rheology: http://www.itconceptfr.com/Pageshtml/Tracker_Desc_VA.html.

[16] Wege, H. A., et al., "Development of a New Langmuir-Type Pendant Drop Film Balance," *Colloids and Surfaces B: Biointerfaces*, Vol. 12, 1999, pp. 339–349.

[17] Berthier, J., et al., "An Analytical Model for the Prediction of Microdrop Extraction and Splitting in Digital Microfluidics Systems," *Proc. Nanotech 2005 Conference,* Anaheim, CA, May 8–12, 2005.

[18] Raccurt, O., J. Berthier, and P. Clementz, "Time Dependent Surface Tension Modification due to Surfactant During Electrowetting Basic Droplet Operation," *Proc. Euromech Colloquium on Microfluidics and Transfer*, Grenoble, France, September 6–8, 2005.

[19] White, S. H., "Small Phospholipid Vesicles: Internal Pressure, Surface Tension, and Surface Free Energy," *Proc. Natl. Acad. Sci. USA,* Vol. 77, No. 7, 1980, pp 4048–4050.

[20] Prange, H. D., "Laplace's Law and the Alveolus: A Misconception of Anatomy and a Misapplication of Physics," *Advan. Physiol. Edu.*, Vol. 27, 2003, pp. 34–40.

[21] Moumen, N., Subramanian R. S., and J. McLaughlin, "The Motion of a Drop on a Solid Surface Due to a Wettability Gradient," *Proc. AIChE 2003 Annual Meeting*, San Francisco, CA, 2003.

[22] Chaudhury, M. K., and G. M. Whitesides, "How to Make Water Run Uphill," *Science*, No. 256, 1992, pp. 1539–1541.

[23] Goldstein, R. J., et al., "Heat Transfer—A Review of 2001 Literature," *Int. J. Heat and Mass Transf.*, Vol. 46, 2003, pp. 1887–1992.

[24] MIT, Lecture 4, Marangoni flows: http://web.mit.edu/1.63/www/Lec-notes/Surfacetension/Lecture4.pdf.

[25] Velankar, S., et al., "CFD Evaluation of Drop Retraction Methods for the Measurement of Interfacial Tension of Surfactants-Laden Drops," *J. Colloid and Interface Science,* Vol. 272, 2004, pp. 172–185.

[26] Colin, S., *Microfluidique*, Paris, France: Hermes Science, 2004.

[27] Hegseth, J. J., N. Rashidnia, and A. Chai, "Natural Convection in Droplet Evaporation," *Physical Review E.,* Vol. 54, No. 2, August 1996, pp. 1640–1644.

[28] Deegan, R. D., "Pattern Formation in Drying Drops," *Physical Review E.*, Vol. 61, No. 1, 2000, pp. 475–485.

[29] Lippmann, G., "Relations Entre les Phénomènes Électriques et Capillaries," *Annales de Chimie et de Physique*, Vol. 5, pp 494–549, 1875.

[30] Pollack, M. G., R. B. Fair, and D. Shenderov, "Electrowetting-Based Actuation of Liquid Droplets for Microfluidic Applications," *Applied Physics Letters,* Vol. 77, No. 11, 2000, pp. 1725–1726.

[31] Cho, S. K., et al., "Splitting a Liquid Droplet for Electrowetting-Based Microfluidics," *Proc. ASME International Mechanical Engineering Congress and Exposition,* New York, November 11–16, 2001.

[32] Moon, H., et al., "Low Voltage Electrowetting-on-Dielectric," *J. Applied Physics,* Vol. 92, No. 7, October 2002, pp. 4080–4087.

[33] Cho, S. K., H. Moon, and C.-J. Kim, "Creating, Transporting, Cutting, and Merging Liquid Droplets by Electrowetting-Based Actuation for Digital Microfluidics Circuits," *J. Microelectromechanical Systems,* Vol. 12, No. 1, 2003, pp. 70–80.

[34] Paik, P., et al., "Electrowetting-Based Droplet Mixers for Microfluidics Systems," *Lab-on-a-Chip*, Vol. 3, 2003, pp. 28–33.

[35] Quilliet, C., and B. Berge, "Electrowetting: A Recent Outbreak," *Current Opinion in Colloid & Interface Science,* Vol. 6, No. 1, 2001, pp. 34–39.

[36] Peykov, V., A. Quinn, and J. Ralston, "Electrowetting: A Model for Contact Angle Saturation," *Colloid Polym. Science,* Vol. 278, 2000, pp. 789–793.

[37] Verheijen, H. J. J., and M. W. J. Prins, "Reversible Electrowetting and Trapping of Charge: Model and Experiments," *Langmuir*, Vol. 15, 1999, p. 6616.

[38] Vallet, M., and B. Berge, "Limiting Phenomena for the Spreading of Water on Polymer Films by Electrowetting," *Eur. Phys. J. B,* Vol. 11, 1999, p. 583.

[39] Berthier, J., et al., "Mechanical Behavior of Micro-Drops in EWOD Systems: Drop Extraction, Division, Motion and Constraining," *Proc. Nanotech 2005 Conference,* Anaheim, CA, May 8–12, 2005.

[40] Shapiro, B., et al., "Equilibrium Behavior of Sessile Drops Under Surface Tension, Applied External Fields, and Material Variations," *J. Applied Physics,* Vol. 93, No. 9, May 2003, pp. 5794–5811.

[41] Bedekar, A. S., J. W. Jenkins, and S. Sundaram, "A Computational Model for the Design of Electrowetting on Dielectric (EWOD) Systems," *Proc. Nanotech 2005 Conference,* Anaheim, CA, May 8–12, 2005.

[42] Duan, R. -Q., S. Koshizuka, and Y. Oka, "Two-Dimensional Simulation of Drop Deformation and Break-Up Around the Critical Weber Number," *Nuclear Engineering and Design,* Vol. 225, 2003, pp. 37–48.